

---

*Research article*

## **Influence of plasma arc characteristics on penetration depth and weld formation during welding of Al-Mg-Mn alloy with asymmetric variable polarity current**

**Volodymyr Korzhyk<sup>1,2</sup>, Andrii Grynyuk<sup>2</sup>, Yunqiang Zhao<sup>1,\*</sup>, Oleksandr Bushma<sup>2</sup>, Oksana Konoreva<sup>2,\*</sup>, Oleksandr Voitenko<sup>2</sup>, Guirong<sup>2</sup> and Zhe Liu<sup>1</sup>**

<sup>1</sup> China-Ukraine Institute of Welding, Guangdong Academy of Sciences, Guangdong Provincial Key Laboratory of Material Joining and Advanced Manufacturing, Guangzhou, 510650, China

<sup>2</sup> E.O. Paton Electric Welding Institute, National Academy of Sciences of Ukraine. 11 Kazymyr Malevych Str., Kyiv, 03150, Ukraine

\* **Correspondence:** Email: zhaoyq@gwi.gd.cn; okskon@meta.ua; Tel: +38-044-205-2516.

**Abstract:** This study investigated the influence of technological parameters of plasma arc welding using a bipolar asymmetric current with a rectangular waveform on weld-pool formation in Al–Mg–Mn alloys, using alloy 1560 containing 6% magnesium as the primary alloying element as the model material. This work established the relative significance of these parameters in governing weld penetration depth. It has been determined that, in addition to the well-known welding parameters (current amplitude and welding speed), weld formation during plasma arc welding with an asymmetric current of reverse polarity is also affected by the frequency of the asymmetric variable-polarity current, the duration of current flow in straight polarity (balance), and the flow rate of the plasma gas. Increasing the plasma gas flow rate (at constant current amplitude, plasma-nozzle orifice diameter, asymmetric variable-polarity current frequency, and balance) leads to an increase in plasma arc voltage of up to 18%, as well as to a corresponding increase in penetration depth. As the frequency of the asymmetric variable-polarity current increases from 50 to 200 Hz, the penetration depth increases by more than a factor of two. Shifting the polarity balance of the asymmetric variable-polarity current toward reverse polarity (from 85% to 50% straight polarity) results in an increase in the average plasma arc voltage, leading to an increase in weld width and an approximately twofold decrease in penetration depth. The use of pure helium as a shielding gas in plasma arc welding with variable-polarity current of aluminum alloys increases the penetration depth by 45%–90% compared with pure argon. Overall, variations in

process parameters during plasma arc welding with asymmetric variable-polarity current exert a significantly stronger influence on weld penetration depth than on weld width.

**Keywords:** aluminum alloy; plasma arc welding; shielding gas composition; frequency of the variable-polarity current; magnitude of the direct polarity fraction; flow rate of the plasma-forming current; welding speed; current strength

---

## 1. Introduction

Plasma-arc welding, in comparison with other arc welding methods such as tungsten inert gas (TIG) and metal inert gas (MIG), presents significant advantages, namely the high temperature in the plasma column (up to 50,000 °C), an energy concentration in the heating spot on the surface of the part that is 5–6 times higher than with TIG, the ability to regulate the value of the welding current independently of the amount of additional metal supplied to the welding zone (in comparison with MIG), and the capability to obtain welds with smaller geometric dimensions and with higher mechanical-strength characteristics [1–3]. The study of the influence of the energy and current-voltage characteristics of the plasma arc, as a concentrated heat source, represents a pertinent task for the development of a broad range of plasma-arc technologies for processing and joining metallic materials, 3D printing of volumetric products, and coating deposition [4,5]. Among the processes for joining metallic alloys, fusion welding of aluminum alloys deserves special attention. This is due to their high thermal conductivity and the rapid formation of an oxide film on their surface, whose melting temperature exceeds that of the base metal [6–9]. Therefore, plasma arc welding, as a concentrated energy source, is particularly suitable for welding these alloys [10,11]. This enables the reduction of residual stresses induced by the overheating of the welded components [12–14]. Welding deformations and residual stresses are among the most complex thermal phenomena arising during the fusion welding process [15–18]. To enhance the efficiency of oxide film removal on the surface of welds in aluminum alloys, it is advisable to employ plasma arc welding with opposite polarity current [19,20]. In this regard, the half-period of straight polarity ensures increased metal melting, while the half-period of reverse polarity facilitates the disruption of the oxide film and cathodic cleaning of the welding zone [21,22].

The application of plasma arc welding enhances both the manufacturing efficiency [23,24] and the strength of welded structures fabricated from aluminum alloys [25–28]. To improve the quality of welded joints, it is possible to optimize welding parameters [29,30], select shielding gases and their mixtures [31,32], modify the weld microstructure [33,34], apply additional technological measures such as welding with current modulation [35–38], and use combined heat sources [39].

The main drawbacks of plasma arc welding of aluminum alloys are the susceptibility to undercut formation in the fusion zone at the upper part of the weld and a somewhat increased likelihood of gas pore formation in the weld metal [40–43]. For example, at identical welding speeds, aluminum alloys alloyed with copper exhibit a greater tendency to form undercuts than alloys alloyed with magnesium [40,44]. To eliminate this defect, welding can be performed with a reduced consumption of plasma-forming gas, which decreases the plasma arc pressure on the weld pool [45]. Horizontal welding, as opposed to vertical welding, helps to prevent undercut at the lower part of the weld [46,47]. Concerning internal pores, they may originate from the presence of non-metallic inclusions [48,49],

evaporation of low-melting-point elements [50,51], and the ingress of hydrogen into the weld pool due to inadequately broken oxide film on the surface [52,53]. Another source of gas porosity is hydrogen dissolved in the base metal during its production. During weld solidification, hydrogen is released and forms gas pores [54,55].

An effective method for eliminating these defects is to analyze the influence of key technological parameters of plasma arc welding on the formation of welded joints in aluminum alloys [56–59].

Asymmetric variable-polarity current (AVPC) holds significant potential for fusion welding of alloys whose surfaces form refractory films (notably aluminum, magnesium, and other light metal alloys) [60–63]. AVPC can be employed both in plasma arc welding (with filler material in the form of wire or granules) and in hybrid processes (arc or laser-arc), sharing a common weld pool. The key advantage of AVPC lies in the flexibility of waveform selection (sine, triangle, or rectangular). The waveform can be independently selected for both the straight polarity (DCEN—direct current electrode negative) and reverse polarity (DCEP—direct current electrode positive) half-cycles. The rectangular waveform is the most effective for breaking the oxide film. Moreover, AVPC with a rectangular waveform, unlike the previously used sinusoidal current at 50 Hz, enables a wide range of continuous frequency variation of the variable-polarity current and smooth adjustment of half-cycle durations during current flow under both DCEN and DCEP polarities. To increase the metal penetration depth and the stability of the tungsten electrode, a longer current flow duration with DCEN is selected, while a longer current flow duration with DCEP is necessary to enhance the efficiency of oxide film removal.

Furthermore, the effective arc length also influences the formation of welded joints. It differs from the actual arc length by the size of the bore channel in the plasma nozzle, as well as by the distance from the inner edge of the plasma nozzle to the tip of the tungsten electrode.

Another parameter influencing the geometry of weld formation in plasma arc welding is the plasma gas flow rate. Furthermore, previous studies have not clarified the relationship between the welding current amplitude and the maximum permissible plasma gas flow rates.

Numerous studies have been conducted on plasma arc welding of aluminum alloys; however, each has addressed only a specific case and focused on investigating an individual phenomenon. In the mid-1980s, the plasma arc welding process was widely employed in the fabrication of structures for the U.S. Space Shuttle program. Plasma arc welding of aluminum alloys was predominantly used in the full-penetration mode of the plasma jet, with the formation of a “keyhole”. Most researchers, including contemporary authors, consider the influence of process parameters in variable-polarity plasma arc welding as factors that affect the stability of keyhole formation, its maintenance during welding, and the production of welded joints without evident formation defects such as undercutting, excessive penetration, and other weld-bead discontinuities. Previous studies [58,64] demonstrated that the amplitude of the current and the DCEN/DCEP ratio influence the stability of the keyhole and weld pool, and therefore the penetration depth and weld-bead geometry. A number of authors have investigated the effects of welding current, welding speed, and arc balance during keyhole plasma arc welding performed in the vertical position [65]. The authors of [66,67] examined the influence of welding current and arc length during the process of plasma powder deposition.

All previous studies addressed specific aspects of weld-pool stability in plasma arc welding with full penetration of the plasma jet (keyhole), or investigated issues related to plasma surfacing using either powder or wire feedstock. A comprehensive investigation of the influence of process parameters under physical modeling of flat-position plasma arc welding of aluminum alloys with bipolar asymmetric (variable polarity) current has not been conducted. Consequently, the relationship between

plasma arc welding parameters and their combined influence on weld geometry during welding of model specimens remains insufficiently understood. The influence of numerous welding process parameters and the mechanisms underlying their effect on the formation and geometric characteristics of the weld have not been addressed at all.

The aim of this study is to establish patterns and elucidate the mechanisms by which the parameters of asymmetric current with a rectangular waveform affect the formation characteristics and geometry of welds during plasma arc welding of the Al–Mg–Mn aluminum alloy. To achieve the stated objective, the following tasks were undertaken:

1. Investigate the current-voltage characteristics of the plasma arc under bipolar current with a rectangular waveform, establish the dependencies of voltage drop on current magnitude and temporal parameters of polarity oscillations, and determine the differences in energy characteristics during half-periods of current flow at DCEN and DCEP polarities.
2. Determine the influence of the effective arc length on arc power, energy concentration in the heating spot, and the geometrical parameters of the welds.
3. Analyze the influence of plasma gas flow rate on the geometrical parameters of welds at different plasma arc current levels.
4. Determine the influence of the frequency of asymmetric variable-polarity current on plasma arc power and weld geometry.
5. Evaluate the effect of current flow duration under straight and reverse polarity on the penetration depth and weld seam width during plasma arc welding of model specimens.
6. Determine the influence of the helium fraction in the shielding atmosphere on the penetration depth and weld width and establish the mechanism underlying this effect.
7. Analyze the effect of welding current amplitude on the penetration depth and weld seam width.
8. To establish the patterns of the effect of welding speed variation on the geometric parameters of the weld seam.

## 2. Materials and methods

Technological studies of plasma arc welding were conducted on flat specimens of the Al–Mg–Mn aluminum alloy system measuring  $200 \times 100 \times 7$  mm (Table 1) [68–71].

**Table 1.** Chemical composition (wt.%) of the 1560 alloy specimens of the Al–Mg–Mn system used in the investigations.

Al	Mg	Mn	Si	Fe	Cu	Zn	Zr	Cr	Ti
Base	5.8–6.8	0.5–0.8	≤0.4	≤0.4	≤0.1	≤0.2	0.02–0.12	–	0.02–0.1

Aluminum alloys with a magnesium content of 4.5%–6.5% are among the most commonly used structural alloys. They are extensively utilized in various branches of mechanical engineering and transportation. Alloys in the Al–Mg–Mn system can be strengthened solely by plastic deformation of semi-finished products during fabrication. Depending on the magnesium content and the degree of plastic deformation, the strength of these alloys (with 4.5%–6.5% magnesium) can range from 300 to 410 MPa. A second advantage of aluminum–magnesium alloys is their high corrosion resistance, not only to fresh water but also to seawater. Moreover, corrosion resistance increases with the magnesium content in the alloy.

This study was conducted using a robotic plasma arc welding system (Figure 1) with asymmetric alternating current [72–76], equipped with an anthropomorphic robot for positioning the welding plasma torch relative to the specimens fixed in the assembly-welding fixture [77–80].

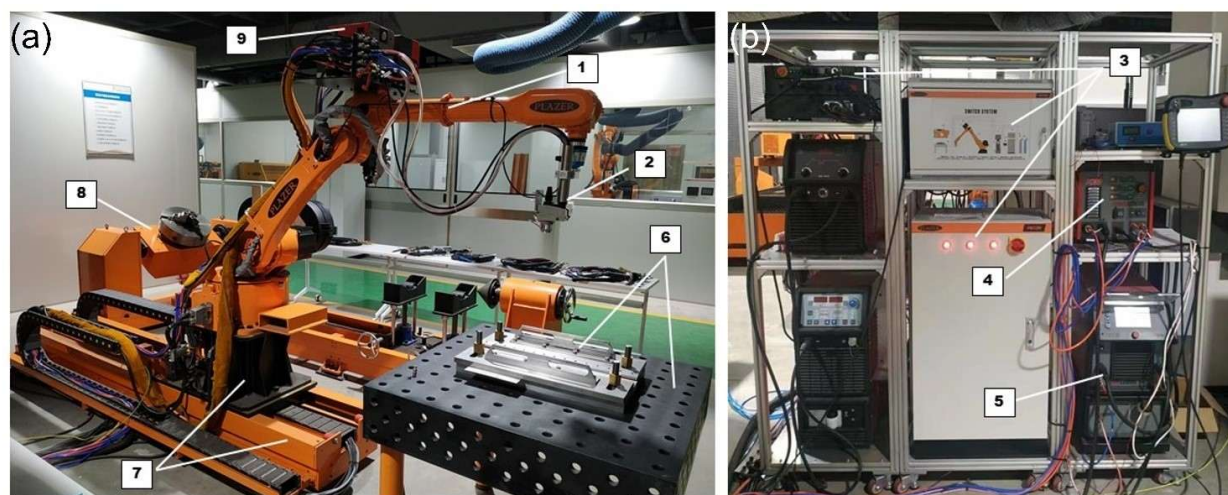


**Figure 1.** (a) General view of the robotic equipment complex for plasma arc welding of long seam joints with asymmetric variable-polarity current (robot arm reaches up to 2000 mm, robot travel system up to 3000 mm), stands with power supplies for the robot, plasma torch, command adaptation cabinet for the robot; and (b) an intelligent automatic monitoring system for welding equipment. 1: welding robot; 2: welding plasma torch; 3: intelligent process control system for robotic welding; 4: plasma module; 5: plasma arc welding power supply; 6: welding table with assembly-welding fixture; 7: robot linear movement system on rails; 8: two-axis rotator-manipulator; 9: filler wire feeding mechanism.

For the investigation of the weldability of selected aluminum alloys across wide ranges of asymmetric alternating current, a PD-174m2 plasma torch (Figure 2) was utilized [81]. This plasma torch is equipped with a set of interchangeable plasma nozzles with orifice diameters ranging from 2.0 to 4.5 mm in 0.5 mm increments. For welding alloys with increased fluidity of liquid metal, plasma nozzles equipped with two or four additional holes of 1.0 mm diameter were utilized. These holes are designed to reduce excessive gas pressure along the nozzle axis and to promote additional elongation of the plasma arc along the weld axis. Furthermore, for efficient operation of the plasma torch within the specified current range, tungsten electrodes with diameters ranging from 3.2 to 6.0 mm were employed. This was achieved by replacing the collet and the washer for supplying electric current to the electrode assembly, as well as the ceramic insulator-centering device made from special heat-resistant ceramic. For welding at high speeds (above 120 cm/min), an additional shielding gas nozzle with a length of 300 mm and a width of 50 mm was attached to the plasma torch.

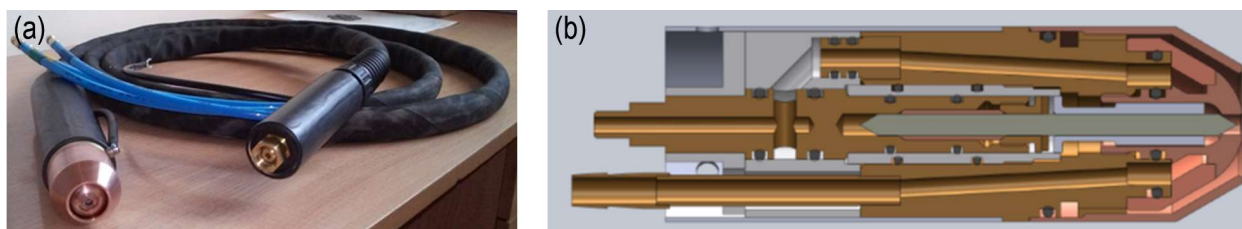


**Figure 2.** (a) External appearance and (b) 3D model cross-section of the PD-174m2 welding plasma torch for welding aluminum alloys with asymmetric opposite polarity current in the welding current range from 80 to 350 A at 100% duty cycle.

Welding was performed without the use of filler wire. The maximum welding current and welding speed were selected to prevent complete penetration of the test specimen. The weld penetration depth and weld width were determined as the average value from a series of five specimens welded under identical parameters. Measurements of the weld geometric characteristics were carried out using a microscope equipped with a digital camera, followed by image processing of the weld cross-sections using specialized software.

Welding was conducted without clamping the specimen. To ensure standardized heat dissipation conditions beneath the specimen, an air gap of at least 20 mm was established. Welds were made along the center of the specimen, following its longitudinal axis. Only one weld bead was made on each specimen. Welding was initiated and terminated at the same distance (15 mm) from each edge of the specimen. After welding, metallographic cross-sections were cut at a distance of 50 mm from the edge of the specimen. The specimen width was 20 mm. Following grinding of the specimens for metallographic examination, chemical etching was performed to reveal the weld structure: etching for 10 min in a 10% aqueous KOH solution, rinsing in running water, brightening in a 30% HNO<sub>3</sub> solution, rinsing in running water, and drying the specimens with hot air.

In plasma arc welding with asymmetric variable-polarity current, two primary types of asymmetry are employed: temporal and amplitude, or solely temporal asymmetry. Temporal asymmetry refers to the difference in the duration of current flow during DCEN and DCEP. Amplitude asymmetry refers to differing amplitude values of current during DCEN and DCEP, with the current amplitude in the reverse polarity typically 30–40 A higher than in the straight polarity. Previous studies conducted at the E.O. Paton Electric Welding Institute have demonstrated that for the high-quality formation of welds in plasma arc welding with variable-polarity current, temporal asymmetry alone is sufficient, provided that the amplitude values of current in both straight and reverse polarities are equal.

All plasma arc welding experiments with variable-polarity current on 7 mm thick Al–Mg samples were conducted using solely the time asymmetry of the variable-polarity current. The current amplitude in straight and reverse polarity was equal.

When investigating the influence of plasma gas flow rates on the geometrical parameters of welds, these increased from a minimum value of 0.2 L/min to the maximum permissible for each current setting in increments of 0.2 L/min. The criterion for halting the increase in gas flow was the formation of surface defects during plasma arc welding, such as deep gas pores, cavities open to the surface, and deep undercuts in the upper portion of the weld. These defects were visually detected either during the welding process or after its completion. Additionally, the maximum permissible gas flow rate was limited by the occurrence of large cavities in the lower sections of the welds, caused by excessive gas pressure.



Before welding, all samples were cleaned of organic contaminants using acetone. Subsequently, chemical etching was performed in an aqueous alkaline solution, followed by brightening in an aqueous nitric acid solution. Mechanical scraping of the sample surfaces was not employed.

Welding was performed using argon (purity 99.998%), pure helium, and argon–helium mixtures as shielding gases. Pure argon 4.8 (99.998% Ar) was used as the plasma-forming gas. Welding was conducted using argon (purity 99.993%) and argon–helium mixtures as plasma and shielding gases.

To investigate the influence of welding parameters on weld formation, welded samples were mechanically sectioned transverse to the weld axis. The current-voltage characteristics of the plasma arc with asymmetric variable-polarity current (rectangular waveform) were examined using a digital oscilloscope that recorded the voltage in both straight and reverse polarity. In subsequent experiments, the average voltage value measured by a voltmeter was employed.

Measurements were conducted using an instrumental microscope with an accuracy of 0.01 mm [82]. Weld quality was assessed according to the ISO 10042 standard (level B) [83]. For other investigations, comprehensive material analysis techniques were applied.

In the course of the investigations presented in this article, no examinations of weld structure or weld mechanical properties were performed.

### 3. Results and discussion

#### 3.1. Current-voltage characteristics of the plasma arc under asymmetric variable-polarity current

The process of plasma arc welding with an asymmetric variable-polarity current, as well as argon arc welding with a non-consumable tungsten electrode, is carried out using power sources with a falling voltage-current characteristic. A change in the amplitude of the welding current causes a directly proportional change in the arc voltage. Furthermore, this characteristic also depends on the arc length.

Previously, due to the complexity of arc ignition during the transition of current from straight to reverse polarity, an additional pulse voltage of several hundred volts was required. Moreover, there was no control over the duration of these pulses. Currently, the rectangular waveform allows the current and voltage curves to cross the zero point almost instantaneously. This reduces the need for additional pulse voltage to just a few volts. The oscillogram of the current and voltage waveforms for this process is shown in Figure 3.

The relationship between the current and the voltage of the plasma arc under asymmetric variable-polarity current is positive: as the welding current increases, the arc voltage also increases. In the range of 100–200 A, an increase in current by 50 A causes the voltage to rise by 1.3 V. In the range of 200–300 A, a comparable increase in current results in a voltage increase of 2.3 V. These values are applicable to both polarities.

As the current increases, the arc voltage rises more rapidly in straight polarity than in reverse polarity. Simultaneously, the difference between these voltages decreases. At a current of 100 A, it is 6.2 V, and at 350 A, it decreases to 4.7 V.

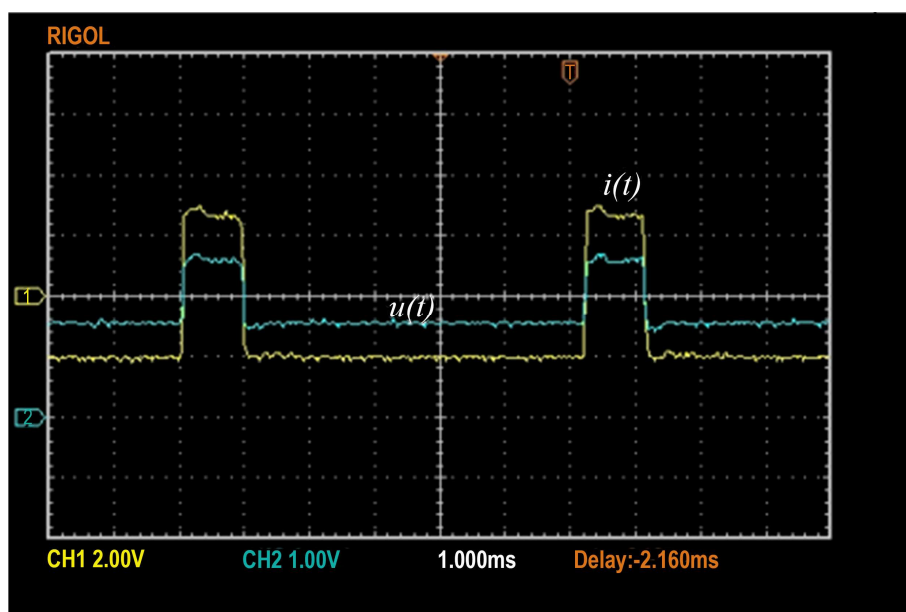


**Figure 3.** Oscillogram of the current and arc voltage curves for a 150 A amplitude rectangular asymmetric variable-polarity current at a frequency of 150 Hz.

Figure 4 shows the current-voltage relationship of the plasma arc welding process with asymmetric variable-polarity current and rectangular waveform under the following conditions: arc length 4.0 mm, argon plasma-forming gas flow rate of 0.4 L/min, and plasma-forming nozzle channel diameter of 4.0 mm.

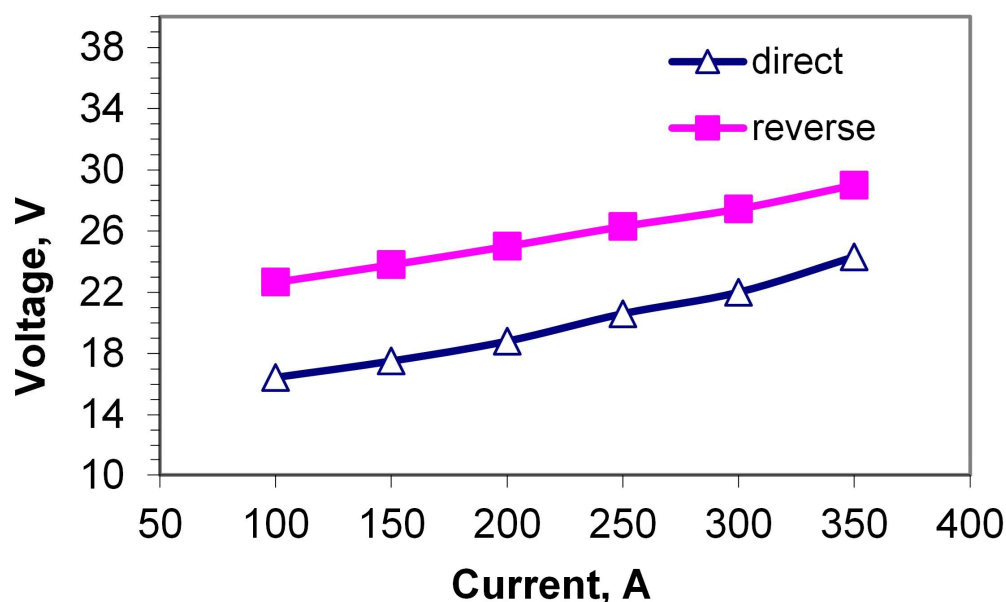


**Figure 4.** Current-voltage characteristics of the plasma arc with asymmetric variable-polarity current for straight and reverse polarity.

The current-voltage characteristics obtained from different plasma torches may exhibit slight variations, specifically differing arc voltages at identical current values. This may be due to differences



in the length of the plasma nozzle channel, which vary among manufacturers despite identical nozzle channel diameters.

The current-voltage characteristic of the plasma arc can be used to calculate plasma arc welding parameters, such as welding speed and welding current amplitude. The methodology for calculating plasma arc welding parameters with asymmetric variable-polarity current is not addressed in this study.

### *3.2. Influence of effective arc length on its energy parameters and metal penetration*

In argon arc welding with a tungsten electrode, the arc length is a key parameter. It influences the arc voltage and power, as well as the energy concentration in the heating zone. By adjusting the arc length, the penetration depth can be effectively controlled, which is particularly important when working with thin metal (0.5–1.0 mm).

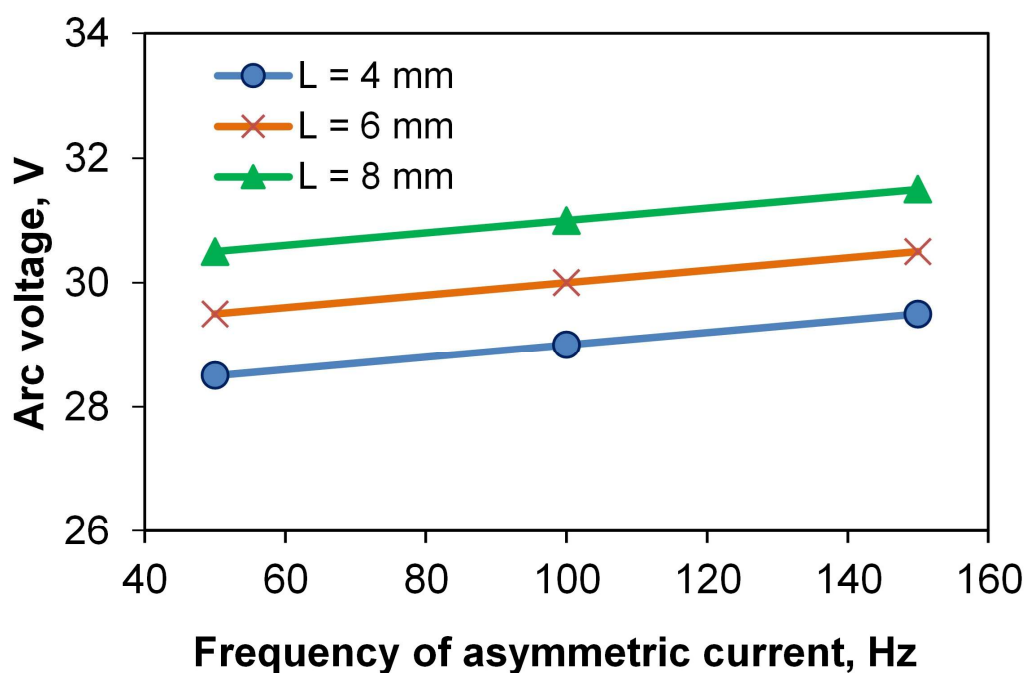
In plasma arc welding of aluminum alloys with asymmetric variable-polarity current, the actual arc length comprises three components: the distance from the tip of the plasma nozzle to the workpiece, the length of the channel within the plasma nozzle, and the distance from the beginning of the channel inside the plasma nozzle to the tip of the electrode. From a technological perspective, when selecting the mode of plasma arc welding, the primary consideration is the distance between the tip of the plasma nozzle and the workpiece. This distance will be designated as the effective arc length. This parameter may vary autonomously during welding due to the deformation of the surfaces of the welded sheets. During the welding process, the length of the plasma nozzle channel and the distance from the electrode to the beginning of the channel within the plasma nozzle remain constant. These parameters are selected based on the design of the plasma torch and the need to ensure stable excitation and maintenance of the plasma arc during welding.

Typically, the length of the plasma nozzle channel is less than or equal to its diameter. The distance between the start of the nozzle channel and the electrode tip may be positive (a gap between the electrode and the plasma nozzle) or negative (the electrode tip is recessed within the plasma nozzle channel).

An investigation of the influence of nominal arc length during plasma arc powder surfacing has been conducted previously [67]. Nevertheless, that study considered a specific case of applying plasma for metal processing, and the use of powder introduced an additional error into the analysis. Our research is aimed at determining the influence of nominal arc length in interaction with other parameters of plasma arc welding using an asymmetric variable-polarity current.

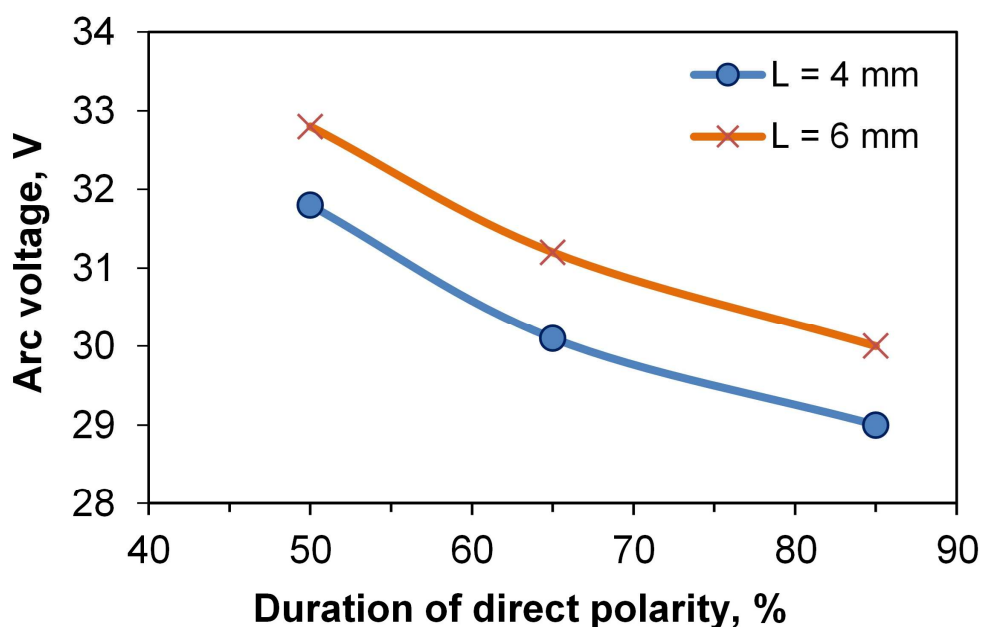
Within the given current range (up to 260 A) and with a tungsten electrode diameter of 4.8 mm, the reduction in the electrode length caused by melting under arc heating is sufficiently small that it can be neglected when measuring the absolute arc length. Therefore, with a constant channel length of the plasma-forming nozzle and a constant distance from the inner surface of the plasma-forming nozzle to the electrode tip, the variable parameter in the experiments is the distance from the electrode tip to the workpiece, i.e., the nominal arc length.

The investigations established that an increase in nominal arc length during plasma arc welding leads to an increase in arc voltage. Figure 5 shows the graph of the change in the average arc voltage (the arithmetic mean of the voltages in straight and reverse polarity) of the plasma arc when welding a 7-mm-thick 1560 aluminum alloy. The experiments were carried out under the following conditions: welding current 260 A, plasma-forming gas flow rate 0.6 L/min, variable-polarity current with 85% straight-polarity duration, and a plasma-forming nozzle channel diameter of 4.0 mm.



**Figure 5.** Plasma arc voltage variation during welding of aluminum alloy 1560 ( $\delta = 7$  mm) as a function of the frequency of asymmetric variable-polarity current and the effective arc length at 85% straight polarity duration.

The average voltage of the plasma arc increases not only with changes in the nominal arc length, but also with variations in the duration of the straight polarity, assuming a constant current frequency, as shown in Figure 6.

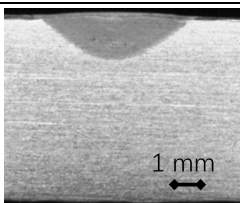
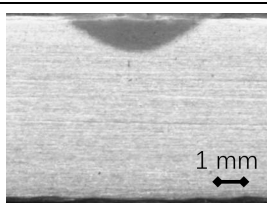
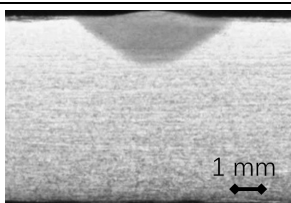
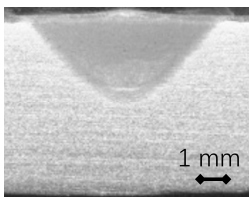
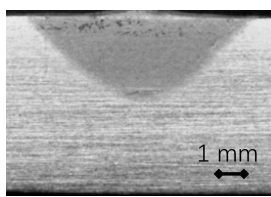
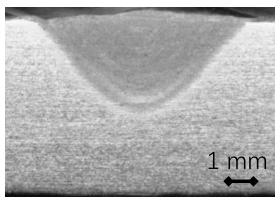


**Figure 6.** Plasma arc voltage variation during welding of aluminum alloy 1560 ( $\delta = 7$  mm) depending on the balance of asymmetric variable-polarity current and nominal arc length at a current frequency of 100 Hz.

The experiments demonstrated a clear trend of an increase in the average plasma arc voltage by 1 V for every 2 mm change in the nominal arc length. Increasing the arc length from 4 to 8 mm during welding of alloy 1560 (Al–Mg–Mn) with a thickness of 7 mm at a current of 180 A does not result in an increase in weld penetration depth (the weld depth remains at approximately 1.5–1.6 mm) (Table 2). Therefore, under these conditions of material thickness, plasma gas flow rate, and welding speed, the arc length does not influence the penetration depth.

When increasing the welding current to 260 A, changes in arc length have virtually no effect on the penetration depth of the welds, provided the plasma gas flow rate remains constant (Table 2). The penetration depth is 3.4–3.5 mm in all trials.

**Table 2.** Appearance of plasma arc penetrations in 1560 alloy plates ( $\delta = 7$  mm) at varying arc lengths  $l_{\text{arc}}$  and current amplitude  $I$  ( $V_{\text{weld}} = 20$  cm/min,  $Q = 0.2$  L/min).

Welding current $I$ , A	Arc length $l_{\text{arc}}$ , mm		
	4	6	8
180			
260			

Increasing the arc length by 100% increases the arc voltage by only 7%. Furthermore, the heating spot enlarges geometrically, with its area increasing by 23%. Simultaneously, the increase in arc power (resulting from the voltage rise) is distributed across a larger heating spot area. This balances the energy concentration in the heating zone per unit area, ensuring that the energy concentration remains almost unchanged, and the weld penetration parameters stay constant. Therefore, within the arc length range of 4–8 mm and at a current between 180 and 260 A, the arc length can be disregarded when selecting parameters for plasma arc welding of aluminum alloys.

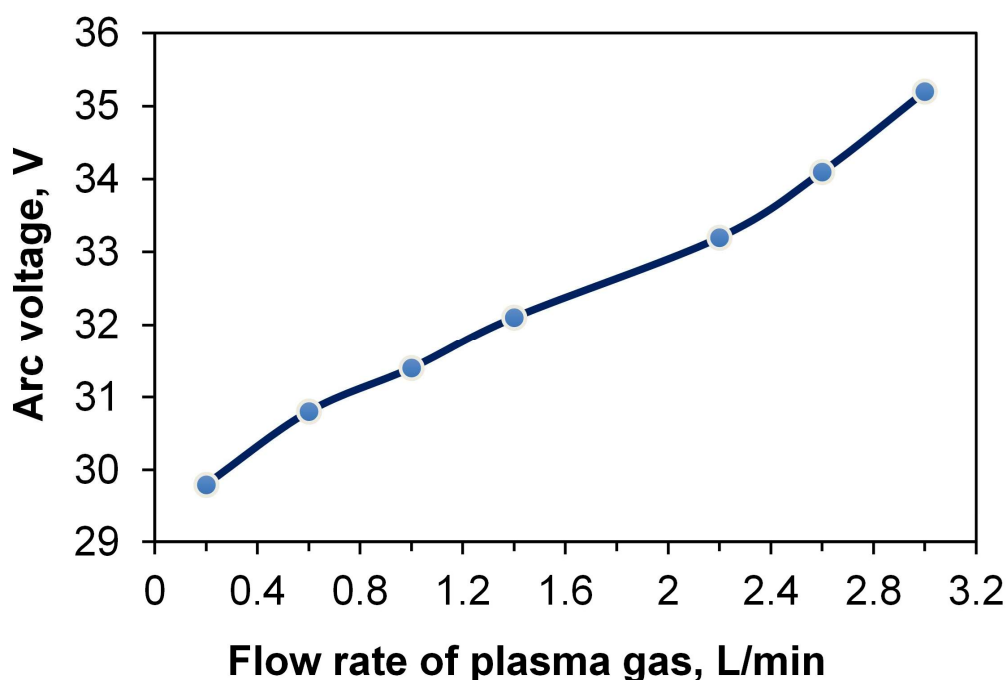
### 3.3. Investigation of the influence of plasma gas flow rates on the geometrical parameters of welds at various plasma arc current values

The authors of [84] investigated the influence of plasma-forming gas flow rate on the stability of bead formation during plasma powder surfacing. They established that there exists a certain limit to increasing the plasma-forming gas flow rate, at which problems in bead shape quality start to occur. Nevertheless, no studies have been carried out to determine the influence of the plasma-forming gas on weld penetration depth and weld width in plasma arc welding of aluminum alloys using an asymmetric variable-polarity current. Therefore, the investigations presented in this section provide an

answer regarding the effect of plasma-forming gas flow rate on changes in the geometric dimensions of the weld, including its combined interaction with other welding parameters.

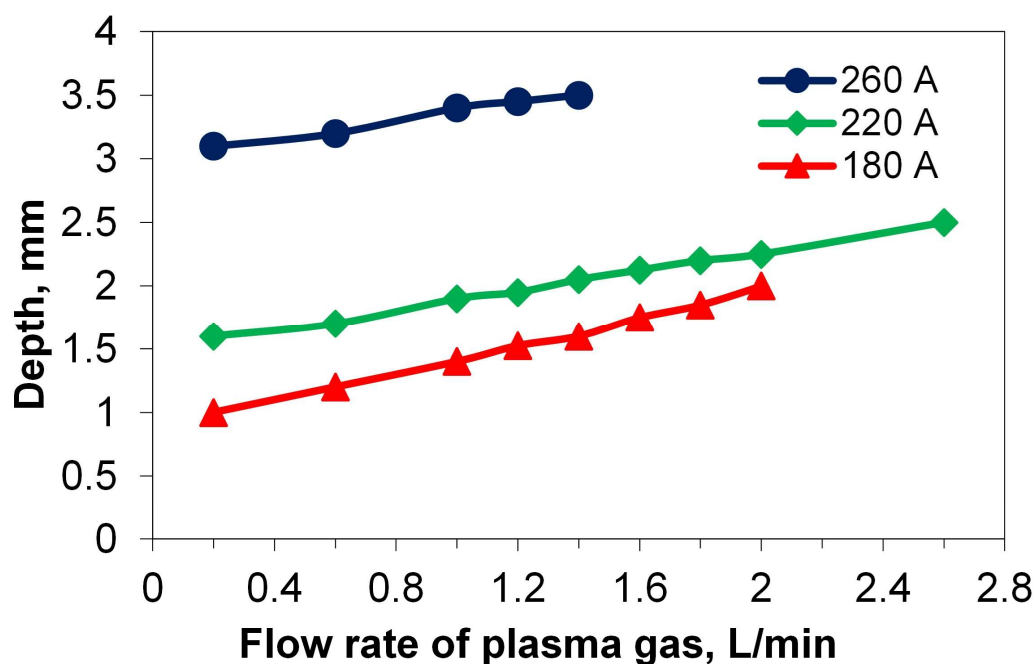
The primary condition for the increase in plasma arc voltage is the enhancement of gas insulation around the plasma column, which restricts its expansion. Figure 7 presents the variation of arc voltage during plasma arc welding with a current of 220 A, an asymmetric variable-polarity current frequency of 100 Hz, a nominal arc length of 6 mm, and a plasma nozzle channel diameter of 3.2 mm. It has been established that with an increase in plasma gas flow rate from 0.2 to 3.0 L/min, the voltage increases by 18%.

High-quality weld formation is achieved only within a specific range of plasma gas flow rates. This range depends on the thickness of the welded metal, the plasma torch travel speed, and the amplitude of the welding current. The conducted studies established the adjustable limits of the plasma gas flow, within which high-quality welds can be obtained, and quantified the influence of changes in these flow rates on the weld penetration depth.



**Figure 7.** Variation of plasma arc voltage during plasma arc welding with asymmetric variable-polarity current depending on plasma gas flow rate.

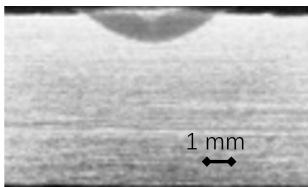
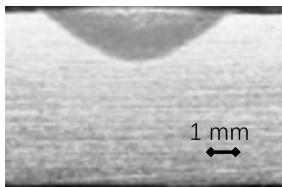
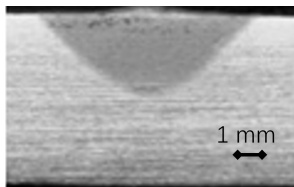
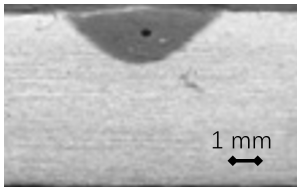
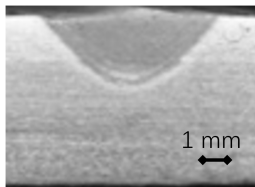
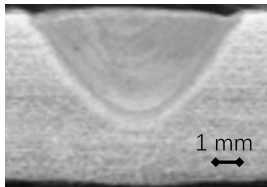
During welding of alloy 1560 (Al–Mg–Mn) with a thickness of 7 mm at a speed of 60 cm/min, the maximum permissible plasma gas flow rates were determined without compromising weld quality (penetration). Process stability was maintained at the following gas flow rates: at a current of 180 A, from 0.2 to 2.0 L/min; at a current of 220 A, up to 2.6 L/min; and at a current of 260 A, up to 1.8 L/min (Figure 8).



**Figure 8.** Effect of plasma gas flow rate on the weld penetration depth during plasma arc welding of alloy 1560 ( $\delta = 7$  mm,  $V_{\text{weld}} = 60$  cm/min;  $l_{\text{arc}} = 6$  mm).

A significant increase in plasma gas flow from 0.2 to 1.8 L/min (an 800% increase) using a welding current of 260 A resulted in only a 19% increase in penetration depth (Table 3). Increasing the plasma gas flow rate during plasma arc welding with asymmetric variable-polarity current results in greater immersion of the plasma jet into the molten metal (Figure 9).

**Table 3.** Appearance of weld penetrations obtained during plasma arc welding of alloy 1560 ( $\delta = 7$  mm) at varying plasma gas flow rates ( $V_{\text{weld}} = 60$  cm/min;  $l_{\text{arc}} = 6$  mm).

Welding current, A	180	220	260
Gas flow rate, L/min	0.2	0.2	0.2
Penetration appearance			
Gas flow rate, L/min	2.0	2.6	1.8
Penetration appearance			

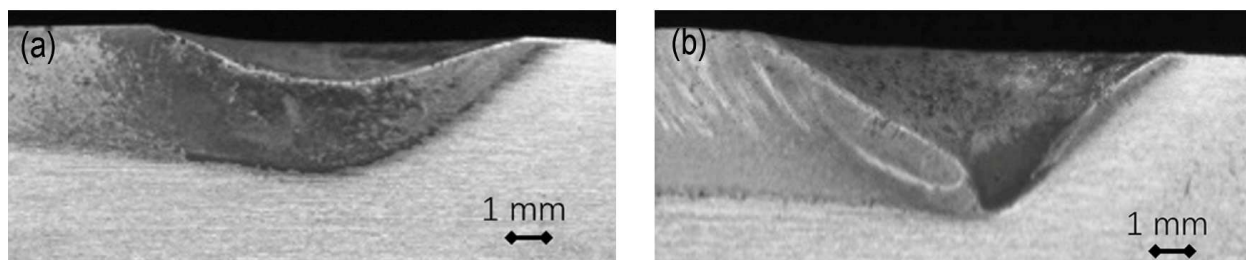


**Figure 9.** Longitudinal macrosections of weld craters obtained by plasma arc welding of alloy 1560 ( $\delta = 7$  mm) at plasma gas flow rates of (a) 0.2 L/min and (b) 1.8 L/min.

Thus, the increase in penetration depth at higher plasma gas flow rates can be attributed to two factors: the increase in plasma arc power due to the rise in arc voltage, and the deeper penetration of the plasma arc into the molten metal of the weld pool. This reduces the thickness of the molten metal layer beneath the arc and enhances the efficiency of heat transfer from the arc to the solid metal.

During plasma arc welding, the molten pool is simultaneously influenced by both the electric arc and the plasma-forming gas. The pressure exerted by the electric arc is proportional to the square of the welding current. Taking this into account, the arc pressure in the current range from 180 to 220 A is 18.8% lower than the arc pressure in the current range from 220 to 260 A. This means that the molten metal pool at a current of 220 A can withstand an additional influence of plasma-forming gas flow rate amounting to 30% more compared with a current of 180 A, and more than 63% compared with a current of 260 A. The increase in the maximum permissible plasma-forming gas flow rate at 220 A compared with 180 A can be explained by the increase in the volume of molten metal; therefore, the pool is capable of withstanding a higher combined pressure of the arc and the plasma-forming gas than a pool of smaller volume, even at a lower welding-current value. Thus, a 1% change in the plasma gas flow rate resulted in a 0.024% change in the sample penetration depth. An 800% increase in the plasma gas flow rate led to the weld width increasing from 8.9 to 9.2 mm during welding at a current of 260 A, representing a 3% increase. Therefore, a 1% change in the plasma gas flow rate corresponds to a 0.004% change in the weld width.

#### *3.4. Determination of the influence of asymmetric variable-polarity current frequency on surface formation quality and weld geometry*

In a previous study [85], the authors presented results on the influence of variable-polarity current frequency during plasma arc welding of aluminum alloys in the keyhole mode. The study showed that the frequency of the variable-polarity current affects the stability of the keyhole during the welding process, in which full penetration through the entire thickness of the welded component was always ensured. Therefore, investigating the influence of variable-polarity current frequency on penetration depth in plasma arc welding is of practical relevance.

Tungsten electrodes of identical diameter were used for the study, along with constant values of frequency and ratio of straight/reverse polarity current duration. The results demonstrated that increasing the frequency of the asymmetric variable-polarity current during plasma welding results in greater penetration depth and reduced weld width. Thus, when performing penetration on alloy 1560, 7 mm thick, using a plasma arc at a speed of 40 cm/min and a current of 260 A, increasing the frequency from 50 to 200 Hz increased the penetration depth from 2.5 to 5.5 mm. Cross-sectional micrographs

of the penetrations illustrating these changes are shown in Figure 10. A further increase in frequency to 240 Hz resulted in complete burn-through of the sample.

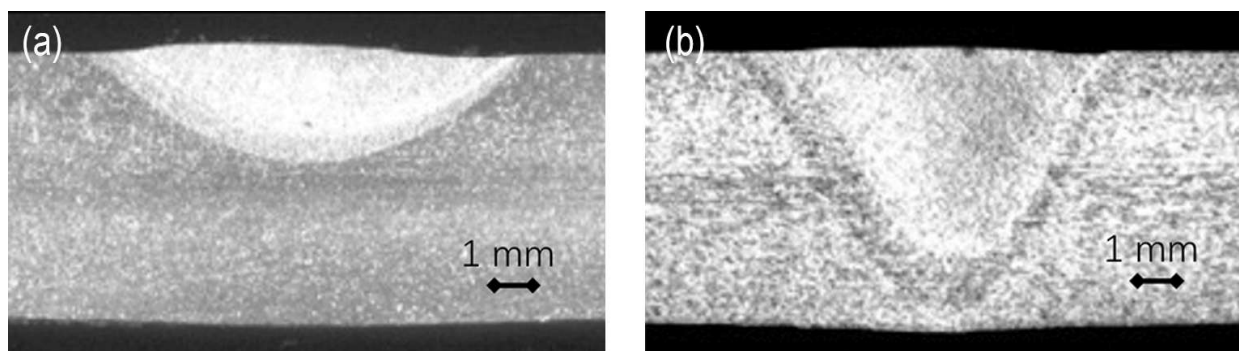


**Figure 10.** Cross-sectional macrostructures of penetrations obtained on alloy 1560 (Al–Mg–Mn) with a thickness of 7 mm by plasma arc welding at a speed of 40 cm/min and a current of 260 A at different frequencies of asymmetric variable-polarity current: (a) 50 Hz,  $\tau_{pr} = 15.6$  ms,  $\tau_{weld} = 4.4$  ms; (b) 200 Hz,  $\tau_{pr} = 3.9$  ms,  $\tau_{weld} = 1.1$  ms.

Changes in current frequency influence both the width and the depth of the weld seam (Figure 11). For example, as the frequency of the asymmetric variable-polarity current increases from 50 to 200 Hz, the weld width decreases from 9.4 to 8.2 mm. Plasma arc welding with asymmetric variable-polarity current is characterized by an increase in arc voltage as the frequency of the asymmetric variable-polarity current increases (Figure 12).

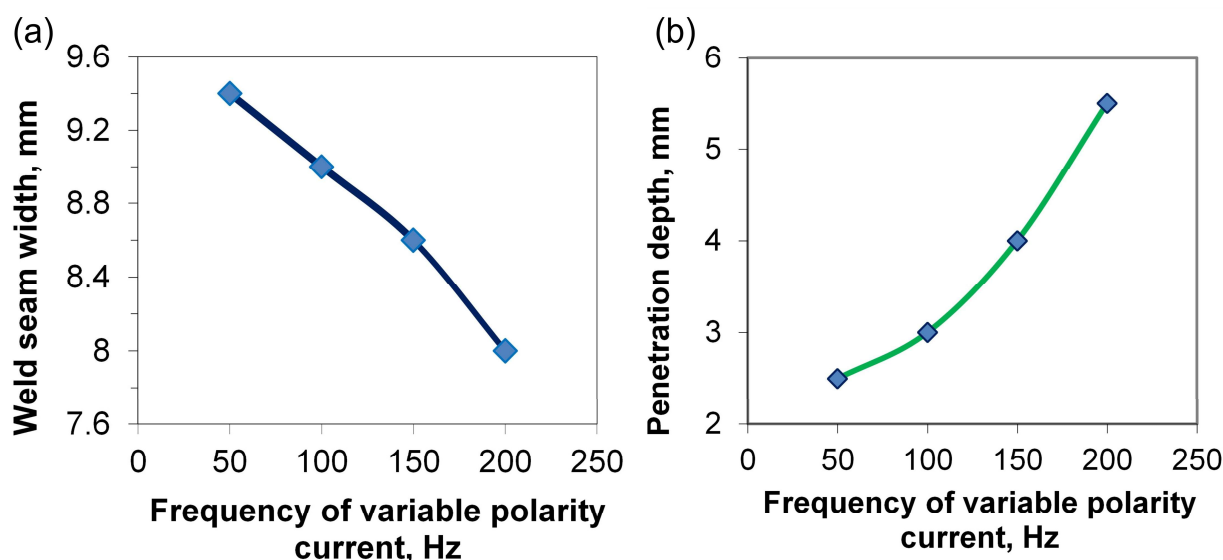


**Figure 11.** Variation of (a) weld width and (b) penetration depth during plasma arc welding of aluminum alloy 1560 ( $\delta = 7$  mm) as a function of the frequency of asymmetric variable-polarity current ( $I_{weld} = 260$  A;  $V_{weld} = 40$  cm/min).

When the frequency of plasma arc welding increases from 50 to 100 Hz, the voltage increases by 0.5–0.6 V (i.e., by 1.7%–1.8%), and the penetration depth of a 7 mm aluminum plate increases



by 20%. Thus, the increase in penetration depth cannot be explained solely by the increase in arc power resulting from the rise in voltage. Simultaneously, a decrease in the weld width is observed.

The reduction in weld width, coupled with the simultaneous increase in penetration depth, indicates enhanced efficiency of energy transfer from the plasma arc to the base metal as the frequency of the asymmetric variable-polarity current increases. This phenomenon can be attributed to the reduction in transition time between the direct and reverse current polarities. Since the arc pressure under straight polarity is somewhat higher compared to reverse polarity, the cumulative force exerted by the arc on the weld pool increases with rising frequency. This results in deeper penetration of the arc into the melt and displacement of the liquid metal, thereby reducing the molten layer beneath the arc. Consequently, heat from the arc is transferred more effectively to the base metal, leading to increased penetration.

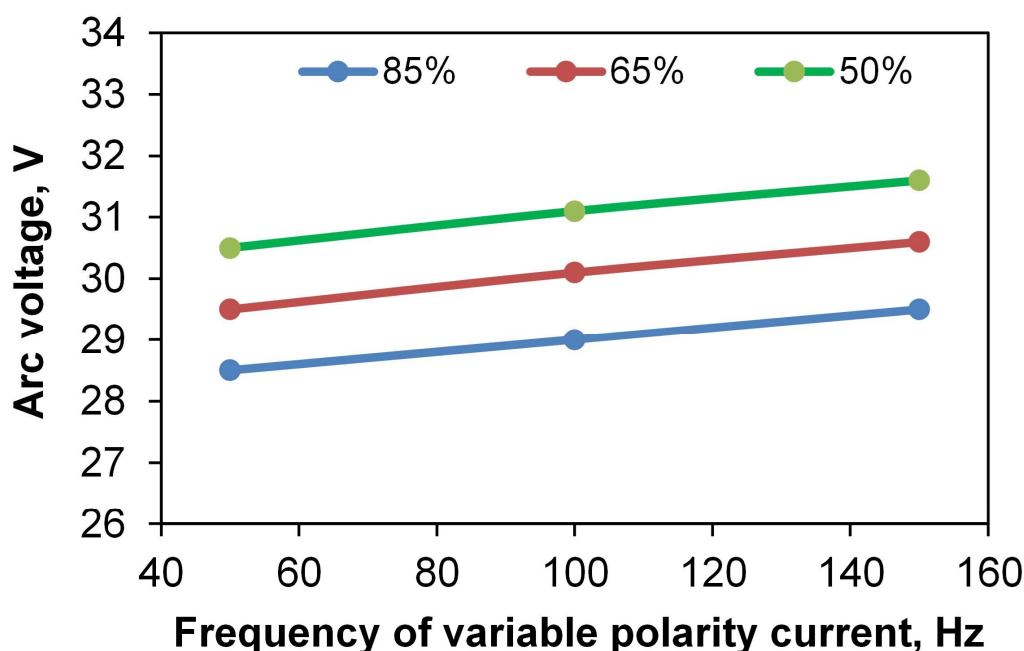


**Figure 12.** Dependence of plasma arc voltage on the frequency of asymmetric variable-polarity current with varying durations of straight polarity current flow during welding ( $I_{\text{weld}} = 250 \text{ A}$ ;  $V_{\text{weld}} = 40 \text{ cm/min}$ ; nominal arc length 4 mm).

Another factor contributing to increased welding efficiency with rising frequency is the reduction in the diameter of the active spot on the weld pool surface. Consequently, the energy concentration in the heating spot increases, facilitating its penetration into the molten metal and, subsequently, an increase in penetration depth.

The increase in arc voltage with rising welding current frequency (at a constant effective arc length) is attributed to the penetration of the plasma arc into the molten metal of the weld pool. This increases the arc length between the electrode and the weld pool surface, resulting in an increase in arc voltage. An increase in the frequency of asymmetric variable-polarity current by 300% leads to a 120% increase in penetration depth. Thus, a 1% change in frequency causes a 0.4% change in penetration depth.

Therefore, increasing the frequency of asymmetric variable-polarity current provides an additional means to enhance weld penetration depth without increasing the current. With a 300% increase in the

frequency of the asymmetric variable-polarity current, the weld width decreased from 9.4 to 8.0 mm, representing a 17.5% reduction. Accordingly, a 1% change in frequency results in a 0.06% change in weld width. Changes in the frequency of the asymmetric variable-polarity current primarily affect the penetration depth of the welds.

### 3.5. Assessment of the influence of current flow duration under straight and reverse polarity on weld formation quality and geometrical parameters

Destruction of the oxide film occurs due to current flow with reverse polarity. At this moment, the workpiece acts as the cathode, and the torch electrode (plasma torch) acts as the anode. Since most of the heat is generated at the anode, excessive heating can cause premature failure of the tungsten electrode.

To reduce thermal impact on the tungsten electrode and prolong its service life without failure, the use of temporal asymmetry—favoring plasma arc burning in direct polarity—was proposed. During the flow of straight polarity current, penetration of the base metal occurs. The majority of heat is generated at the anode, which is the welded metal. To ensure effective disruption of the oxide film and reduce thermal loading on the electrode, the duration of current flow at reverse polarity is minimized (for example, to 3–4 ms).

The arc voltage at reverse polarity is higher than at straight polarity under identical current intensity and plasma gas flow conditions. By adjusting the balance (the ratio of current flow duration between straight and reverse polarity), the plasma arc power can be modified due to the higher voltage at reverse polarity (Figure 13).

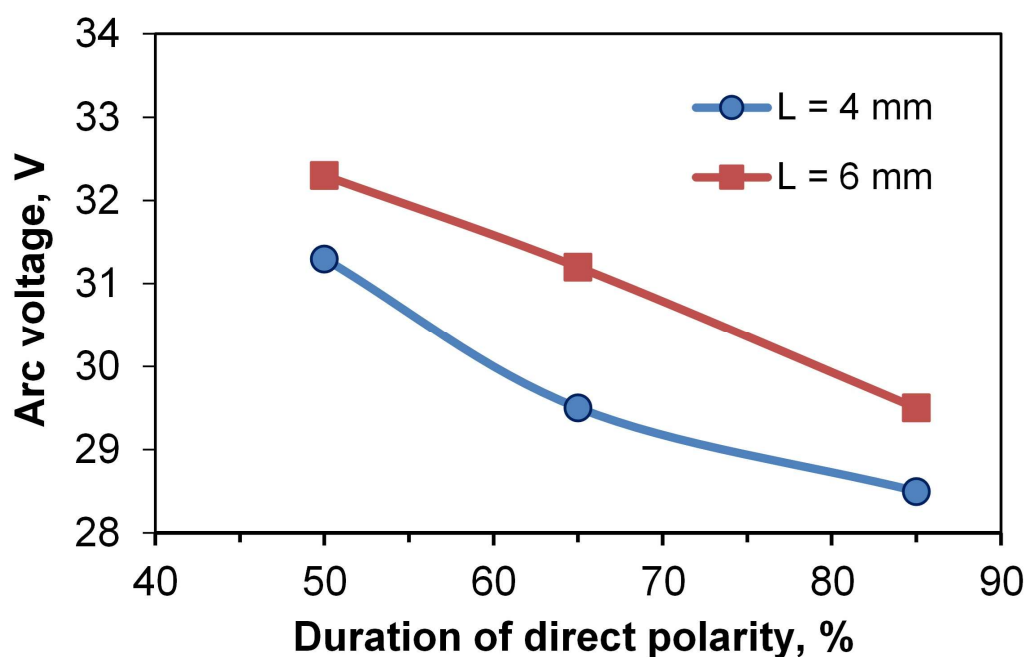


**Figure 13.** Variation of plasma arc voltage depending on the polarity balance of asymmetric variable-polarity current and nominal arc length during plasma arc welding of aluminum alloy 1530 ( $\delta = 7$  mm) at an asymmetric variable-polarity current frequency of 50 Hz.

It was established that increasing the fraction of straight polarity during the welding cycle reduces the average arc voltage. This trend is observed not only at an asymmetric variable-polarity current frequency of 100 Hz (Figure 14) but also at 150 Hz (Figure 15) and other higher frequencies.

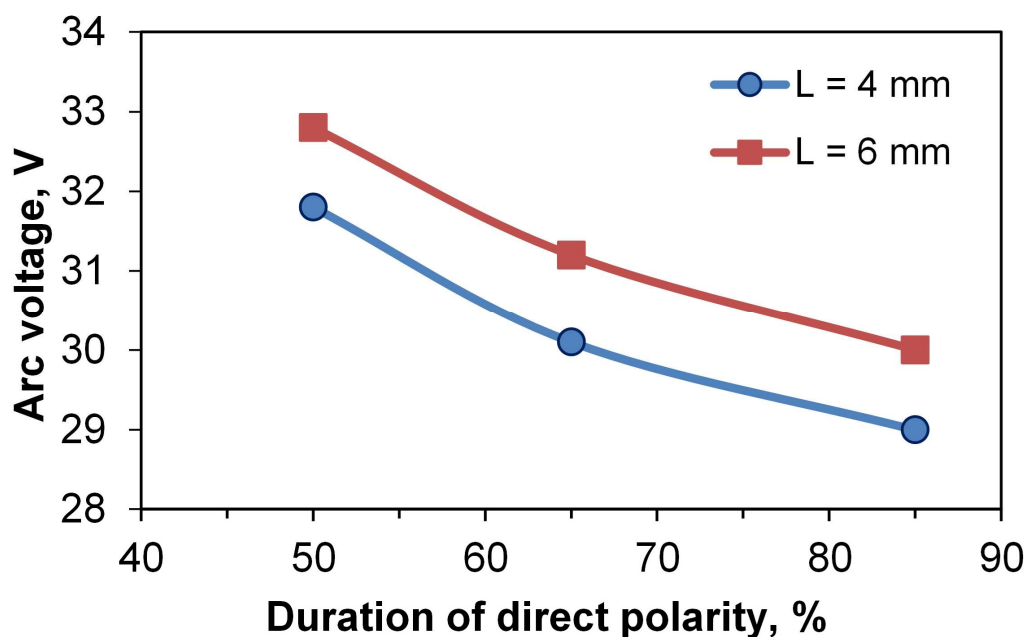


**Figure 14.** Variation of plasma arc voltage depending on the polarity balance of the asymmetric variable-polarity current and the effective arc length during plasma arc welding of aluminum alloy 1560 ( $\delta = 7$  mm) at a frequency of 100 Hz.

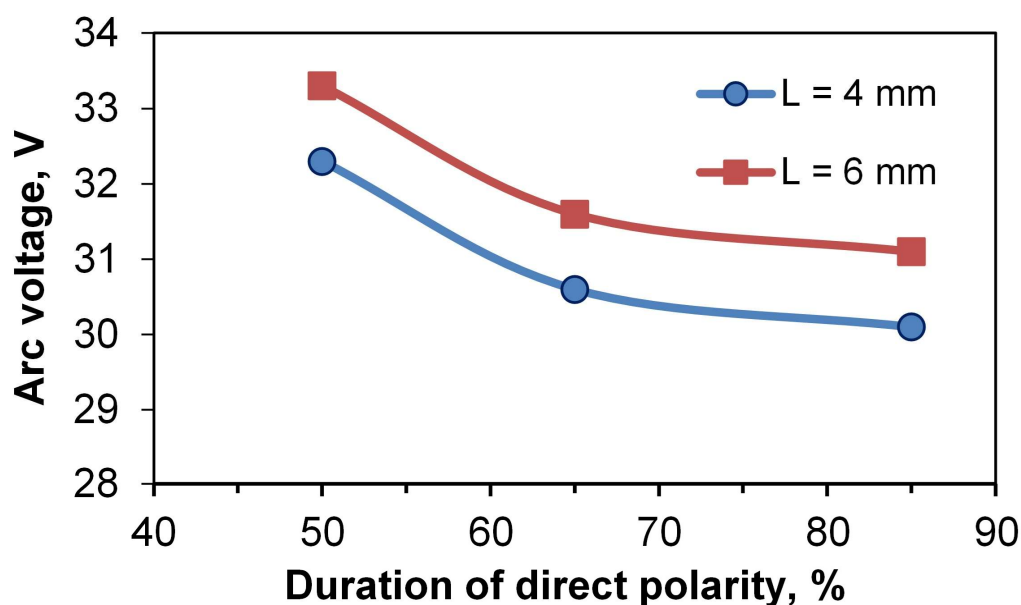


**Figure 15.** Variation of plasma arc voltage depending on the polarity balance of the asymmetric variable-polarity current and the effective arc length during plasma arc welding of aluminum alloy 1530 ( $\delta = 7$  mm) at a frequency of 150 Hz.

The influence of the polarity balance of the asymmetric variable-polarity current on the geometric dimensions of the welds was also investigated. The welds were produced by plasma welding with asymmetric variable-polarity current at a constant current of 260 A, a plasma gas flow rate of 0.6 L/min, an arc length of 6 mm, and a welding speed of 40 cm/min. The frequency of the asymmetric variable-polarity current was constant at 200 Hz.

The study established that the maximum penetration depth occurs at an asymmetric variable-polarity current balance of 85% straight polarity (Figure 16a). As the proportion of reverse polarity increases toward 65% straight polarity, the penetration depth decreases, while the weld width slightly increases (Figure 16b). When the durations of direct and reverse polarity are equal, the penetration depth decreases compared to the 65% straight polarity balance and reaches only 50% of the penetration depth observed at the 85% straight polarity balance (Figure 16c).

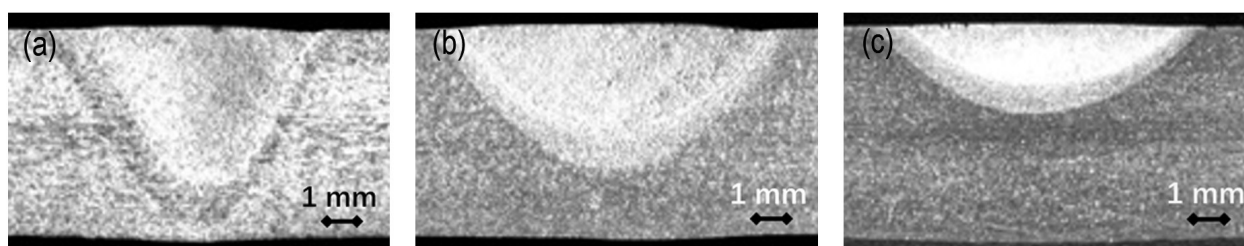


**Figure 16.** Cross-sections of penetration profiles obtained in a 1530 alloy plate by plasma arc welding with asymmetric variable-polarity current at different durations of straight polarity current flow: (a) 85%, (b) 65%, and (c) 50%.

With reversed polarity, noticeably larger geometric dimensions of the arc column are observed compared to those with straight polarity. This leads to a reduction in penetration depth during plasma arc welding as the proportion of reverse polarity increases. Such a reduction in penetration depth may indicate a decrease in the pressure exerted by the plasma jet on the molten metal of the weld pool. This results in a decreased impingement of the jet into the molten metal of the weld pool, an increased layering of liquid metal beneath the plasma jet, and, consequently, a reduction in the efficiency of heat transfer from the plasma jet to the unmelted metal. Thus, the reduction of plasma jet pressure on the molten pool under reverse polarity results in a decrease in weld penetration depth. At the same time, the increase in weld width is attributed to the rise in arc power caused by an increase in the average voltage under reverse polarity.

Therefore, to increase the penetration depth while maintaining other plasma arc welding parameters constant, an additional approach is to shift the balance of the asymmetric alternating current toward current flow under direct polarity. A 35% reduction in the duration of current flow under direct polarity results in a decrease in penetration depth from 5.5 to 2.4 mm (a reduction of 3.1 mm), which corresponds to 129% relative to the final value. A 1% change in the duration of current flow under direct polarity causes a 2.58% change in penetration depth.

The weld width increases from 8.0 to 9.35 mm with a reduction in the duration of current flow under straight polarity, representing a 17% increase. A 1% change in the duration of current flow under straight polarity results in a 0.34% change in weld width.

Changes in the duration of current flow under straight polarity have a greater impact on penetration depth than on weld width.

### 3.6. Influence of helium content in the shielding atmosphere on weld formation

Helium as a shielding gas has been widely used in TIG welding, including the welding of aluminum alloys. Thus, in [86], the authors investigated the effect of helium used as a shielding gas on weld formation, including its influence on penetration depth. Therefore, the investigation of the influence of pure helium, as well as mixtures of argon and helium, on weld penetration depth and weld width during plasma arc welding with an asymmetric variable-polarity current is relevant.

Using helium as a shielding gas instead of argon increases the arc's penetration capability. Thus, for the 1560 alloy with a thickness of 7 mm, the weld width increased from 9.7 to 12.4 mm, and the penetration depth increased from 2.8 to 4.8 mm at a welding speed of 60 cm/min and a welding current of 220 A (Figure 17). Helium possesses a higher ionization potential, resulting in an increase in arc voltage by 1.5–2 times compared to welding in argon at identical welding current values.

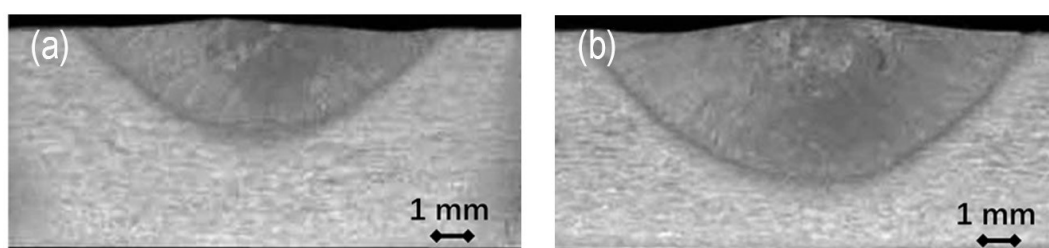


**Figure 17.** Transverse macrosections of penetration welds in alloy 1560 ( $\delta = 7$  mm) obtained by plasma arc welding at a travel speed of 60 cm/min and a current of 220 A with shielding by (a) argon and (b) helium.

Thus, the use of 100% argon (Ar) as the shielding gas resulted in a 71% increase in penetration depth when employing a plasma arc with asymmetric variable-polarity current, while all other welding parameters remained constant. Figure 18 shows the cross-sections of welds in the aluminum–magnesium alloy 1560 ( $\delta = 7$  mm), produced by plasma arc welding at a speed of 60 cm/min with current under shielding gases of 25% Ar + 75% He (Figure 18a), 50% Ar + 50% He (Figure 18b), and 75% Ar + 25% He (Figure 18c).

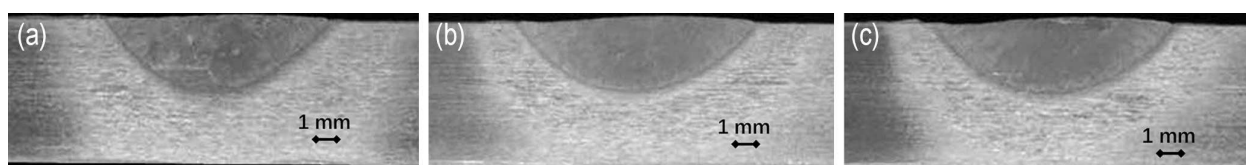


**Figure 18.** Cross-sectional macrographs of penetrations in the 7 mm thick 1560 alloy (Al–Mg–Mn), produced by plasma arc welding at a speed of 60 cm/min using various shielding gas compositions: (a) 25% Ar + 75% He, (b) 50% Ar + 50% He, and (c) 75% Ar + 25% He.

The use of various argon–helium mixtures for shielding the welding zone (75% Ar + 25% He, 50% Ar + 50% He, and 25% Ar + 75% He) leads to an increase in weld penetration depth from 3.0 to 4.0 mm, representing a 0.66% increase in penetration depth with the increase in helium content in the argon–helium mixture (Figure 18).

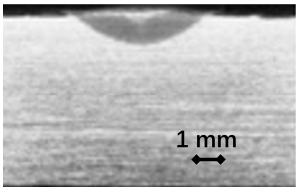
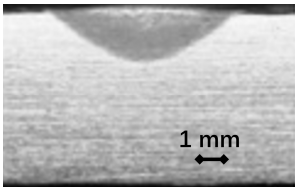
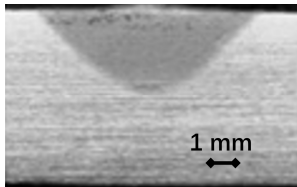
Despite the fact that helium improves the spreading behavior of the filler metal and increases the penetration depth without the need to raise the welding current, it presents disadvantages, such as its significantly higher cost and a much shorter electrode service life (compared with argon, by at least a factor of 3–5).

To reduce the costs associated with expensive helium, the authors of [72] investigated the efficiency of employing a helium–neon mixture as a shielding gas. This mixture constitutes an intermediate product in the process of obtaining pure helium and neon, and its cost is considerably lower.

### 3.7. Determination of the influence of welding current amplitude variation on the geometrical parameters of welds

An increase in the amplitude of the welding current results in a significant increase in the penetration depth of welds (Table 4).

**Table 4.** Appearance of penetrations obtained during plasma arc welding of alloy 1560 (Al–Mg–Mn) ( $\delta = 7$  mm) with different values of welding current ( $V_{\text{weld}} = 60$  cm/min;  $l_{\text{arc}} = 6$  mm).

Welding current, A	180	220	260
Gas flow rate, L/min	0.2		
Penetration appearance			

During welding of alloy 1560 (Al–Mg–Mn) with a thickness of 7 mm, under identical arc length, plasma-forming gas flow rate, frequency and polarity balance of asymmetric variable-polarity current, and welding speed, the penetration depth increases from 1.9 to 3.7 mm (by 95%) with a 44% increase in welding current amplitude. Thus, a 1% change in welding current results in a 2.14% change in penetration depth.

The weld width increased from 4.19 to 7.20 mm (by 73%) as the current rose from 180 to 260 A. In percentage terms, the increase in current caused a greater increase in penetration depth (95%) than in weld width (73%). A 1% change in welding current causes a 1.67% change in weld width.

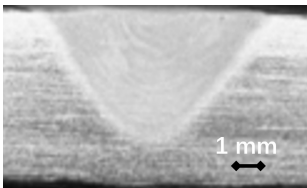
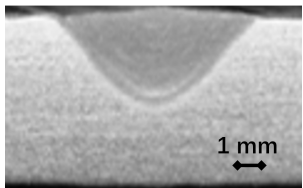
### 3.8. Determination of the effect of welding speed variation on the geometrical parameters of welds

Welding speed is an important parameter to the plasma arc welding process using an asymmetric variable-polarity current for aluminum alloys. Nevertheless, in previous studies by other authors, no analysis was presented regarding the influence of welding speed specifically on weld penetration depth; instead, the influence of welding speed on weld width was evaluated, because the assessment involved not a model specimen but a finished welded joint that was always fully penetrated through its entire thickness [87]. To determine the nature of the effect of changes in welding speed, expressed numerically, on penetration depth, penetration welds were produced on 7-mm-thick sheets of the

aluminum–magnesium alloy 1560 (Al–Mg–Mn) at a welding current of 260 A and at three different welding speeds (50, 60, and 70 cm/min), while keeping all other welding parameters constant. Table 5 shows cross-sectional micrographs obtained by plasma arc welding of sheets made from this alloy at a current of 260 A and the specified welding speeds.

Reducing the plasma torch travel speed from 60 to 50 cm/min (by 20%) during welding of alloy 1560 (Al–Mg–Mn) with a thickness of 7 mm at a current of 260 A resulted in an increase in penetration depth from 3.7 to 5.0 mm (by 35%). The same tendency of decreasing weld width and penetration depth is observed when the welding speed is reduced from 70 to 60 cm/min. An inverse relationship is observed: an increase in welding speed, with all other welding parameters remaining constant, leads to a decrease in weld width and penetration depth. Thus, a 1% change in welding speed results in a 1.75% change in penetration depth. When decreasing the welding speed from 60 to 50 cm/min, the weld width increased from 6.8 to 7.2 mm, representing a 5.9% increase. Therefore, a 1% change in welding speed leads to only a 0.3% change in weld width.

**Table 5.** Appearance of penetration welds obtained by plasma arc welding of alloy 1560 ( $\delta = 7$  mm) at the same welding current of 260 A and at different welding speeds ( $V_{\text{weld}} = 50$  and 60 cm/min).

Welding speed, cm/min	50	60
Penetration appearance		

Hence, the analysis of the research results demonstrated that during plasma arc welding with asymmetric variable-polarity current, exemplified by the studied Al–Mg–Mn alloy system, variations in welding process parameters such as welding current amplitude, variable-polarity current frequency, welding speed, variable-polarity current balance, and plasma gas flow rate influence penetration depth more significantly than weld width.

In terms of their influence on the penetration depth, the parameters of plasma arc welding with asymmetric variable-polarity current can be prioritized in the following sequence:

1. The duration of current flow under straight polarity: a 1% change in this parameter results in a 2.58% change in penetration depth.
2. The amplitude of the welding current: a 1% change in this parameter results in a 2.14% change in penetration depth.
3. Welding speed: a 1% change in welding speed results in a 1.75% change in penetration depth.
4. Frequency of variable-polarity current with opposite polarity: a 1% change in this parameter causes a 0.4% change in penetration depth.
5. Consumption of plasma gas: a 1% change in plasma gas consumption results in a 0.024% change in penetration depth.

The above sections presented the maximum possible values of welding parameters that ensure the greatest penetration of the specimen; however, when welding an actual joint, their mutual interaction must be taken into account, and the recommendations regarding the selection of welding parameters will take the following form:



1. The welding current will depend on the thermophysical properties of the material and the desired welding speed; under real conditions, it will be limited by the technical capabilities of the power source and the maximum power of the plasma torch (for alloy 1560 with a thickness of 7 mm at a welding speed of 80 cm/min, the welding current will be 460–465 A).

2. The welding speed for each alloy will be limited by the maximum possible welding current, and in some cases, the welding speed will also be limited by the risk of undercut formation in the upper part of the weld bead. Such a risk may occur when welding alloys containing 6% magnesium at speeds above 60 cm/min. For alloy 1560 with a thickness of 7 mm, a welding speed of 80 cm/min is attainable at currents up to 465 A.

3. The current balance (the ratio between the duration of the electrode-negative and electrode-positive polarities) should not be less than 75% in order to improve the stability of the tungsten electrode and ensure effective disruption of the oxide film on the surface of the welded components.

4. When selecting the variable-polarity current frequency, it is also necessary to consider the technical capabilities of the welding power source, as well as the fact that at frequencies above 150 Hz, the constricted arc becomes so highly concentrated in energy that a sharp transition from the weld to the base metal is observed in the upper part of the weld, which adversely affects joint stability under cyclic loading. Therefore, a variable-polarity current frequency of 150 Hz is recommended.

5. The nominal arc length, although it does not significantly influence penetration depth or weld width (as opposed to the TIG process), does affect the formation of the upper part of the weld when welding with a filler wire. Thus, for welding alloy 1560 with a thickness of 7 mm, the recommended nominal arc length is 6 mm.

6. The plasma-forming gas flow rate is closely dependent on the welding current. To reduce the total pressure on the molten metal in the weld pool, it is recommended to decrease the plasma-forming gas flow rate as the welding current increases to 460–465 A. If at welding currents up to 300 A, the recommended plasma-forming gas flow rate is 0.5–0.6 L/min, then at currents in the range of 450–475 A, the recommended flow rate is 0.3–0.4 L/min.

These recommendations for the preliminary selection of parameters for plasma arc welding with an asymmetric variable-polarity current are provided for the case of welding in the flat position with filler-wire feeding and with root-bead formation using a backing plate with a forming groove.

#### 4. Conclusions

1. In plasma arc welding with asymmetric variable-polarity current in the range of 100–350 A, the arc voltage exhibits an increasing current-voltage characteristic. This indicates that, with constant parameters (nominal arc length, current frequency, ratio of straight to reverse polarity duration, plasma gas flow rate), an increase in welding current results in a proportional increase in arc voltage. Therefore, the increase in penetration with rising current is attributable not only to the enhanced plasma arc power due to the increased current but also to an additional increase resulting from the rise in arc voltage.

2. It was established that varying the nominal arc length from 4 to 8 mm during plasma arc welding with asymmetric variable-polarity current at current values between 180 and 260 A practically does not affect the weld penetration depth. Therefore, variations in the nominal arc length within this range during welding at the specified current values can be disregarded.

3. It was established that increasing the flow rate of the plasma gas during plasma arc welding with asymmetric variable-polarity current of aluminum alloys, while maintaining constant current

intensity, plasma nozzle channel diameter, and frequency and balance of the variable-polarity current, results in an increase in the plasma arc voltage by up to 18% and a corresponding increase in penetration depth. The latter is determined by two factors: an increase in plasma arc power due to the rise in voltage and an intensified mechanical effect on the molten metal in the weld pool exerted specifically by the gas component. A higher-velocity gas flow immerses the plasma jet into the molten metal, reducing the layer of molten metal beneath the plasma flow and thus enhancing the efficiency of heat transfer to the unmelted metal. The maximum permissible plasma gas flow rates that ensure the high-quality formation of the weld seam depend on the amplitude of the welding current and the volume of molten metal in the weld pool; with an increase in current amplitude, the maximum permissible plasma gas flow rates decrease. Specifically, a 1% change in the plasma gas flow rate results in a 0.024% change in the specimen's penetration depth, whereas the weld width changes by 0.004%.

4. It has been established that during plasma arc welding of aluminum alloys, the penetration depth increases by more than twofold as the frequency of asymmetric variable-polarity current rises from 50 to 200 Hz. This increase occurs most rapidly within the range of 100 to 150 Hz. Simultaneously, the weld width decreases. Therefore, a 1% change in the frequency of asymmetric variable-polarity current results in a 0.4% change in penetration depth, while the change in weld width is 0.06%.

5. When the balance of asymmetric variable-polarity current shifts toward reverse polarity (changing from 85% to 50% straight polarity), the average voltage value of the plasma arc increases. This occurs due to an increased proportion of reverse polarity current, which exhibits a higher voltage value than the straight polarity current. The trends in weld penetration depth and width relative to the balance of asymmetric variable-polarity current are observed throughout the investigated frequency range of 50–200 Hz. A 1% change in the duration of current flow at straight polarity results in a 2.58% change in penetration depth, while the change in weld width is 0.34%.

6. The use of pure helium as a shielding gas in plasma arc welding of aluminum alloys with opposite polarity current enables an increase in penetration depth by 45%–90% compared to the use of pure argon. This enables an increase in the technological capabilities of the plasma arc without raising the current load on the plasma nozzle and the tungsten electrode of the plasma torch.

7. It has been established that during plasma arc welding with asymmetric variable-polarity current, increasing the current intensity within the range of 180–260 A leads to an increase in both weld width and penetration depth. A 1% variation in welding current results in a 2.14% variation in penetration depth, while the weld width varies by 1.67%.

8. Reducing the welding speed, while keeping all other parameters of plasma arc welding with asymmetric variable-polarity current unchanged, leads to an increase in the geometric dimensions of the weld. A 1% change in welding speed results in a 1.75% change in penetration depth, while the weld width varies by 0.34%.

### **Use of AI tools declaration**

The authors declare they have not used Artificial Intelligence (AI) tools in the creation of this article.

## Acknowledgments

The research was funded within the following programs:

1. The GDAS'Project of Science and Technology Development (2020GDASYL-20200301001), China. Note: This project is a strategic project of Guangdong Provincial Academy of Sciences.
2. National Key Research and Development Program of China (Project Number: 2020YFE0205300). Note: This project is part of the “One Belt, One Road” joint laboratory.

## Author contributions

Volodymyr Korzhyk, Yunqiang Zhao: general research management, work ideology; Oleksandr Bushma, Oleksandr Voitenko, Andrii Grynyuk: research methodology, conclusions; Oksana Konoreva, Guirong: conducting technological and metallographic studies; Andrii Grynyuk, Zhe Liu, Oleksandr Voitenko: processing of results, writing the article.

## Conflict of interest

The authors declare no conflict of interest.

## References

1. Lee G, Kim H, Jeon J, et al. (2023) Development of plasma arc spot welding process and finite element method analysis model for predicting fracture strength: Part 1—Development of plasma arc spot welding process. *Int J Precis Eng Manuf* 24: 1–11. <https://doi.org/10.1007/s12541-022-00707-1>.
2. Lee G, Kim H, Jeon J, et al. (2023) Development of plasma arc spot welding process and finite element method analysis model for predicting fracture strength: Part 2—Development of finite element method analysis model for predicting fracture strength. *Int J Precis Eng Manuf* 24: 13–23. <https://doi.org/10.1007/s12541-022-00706-2>
3. Gulyaev IP, Dolmatov AV, Kharlamov MY, et al. (2015) Arc-plasma wire spraying: An optical study of process phenomenology. *J Therm Spray Tech* 24: 1566–1573. <https://doi.org/10.1007/s11666-015-0356-6>
4. Borisov Y, Korzhyk V, Revo S (1998) Electric and magnetic properties of thermal spray coatings with an amorphous structure. *Proc Int Therm Spray Conf* 1: 687–691. <https://doi.org/10.31399/asm.cp.itsc1998p0687>
5. Xu S, Deng X (2004) An evaluation of simplified finite element models for spot-welded joints. *Finite Elem Anal Des* 40: 1175–1194. <https://doi.org/10.1016/j.finel.2003.08.006>
6. Li Y, Zou W, Lee B, et al. (2020) Research progress of aluminum alloy welding technology. *Int J Adv Manuf Technol* 109: 1207–1218. <https://doi.org/10.1007/s00170-020-05606-1>
7. Wu B, Krivtsun IV (2019) Processes of nonconsumable electrode welding with welding current modulation (Review). Part 1. Peculiarities of burning of nonstationary arcs with refractory cathode. *Avtomat svarka* 11: 29–39. <https://doi.org/10.15407/as2019.11.05>

8. Wu B, Krivtsun IV (2019) Processes of nonconsumable electrode welding with welding current modulation (Review). Part II. Effects of arc impact on the metal being welded. *Paton Weld J* 12: 11–23. <https://doi.org/10.15407/tpwj2019.12.02>
9. Silva D, Scotti A (2016) Using either Mean or RMS values to represent current in modeling of arc welding bead geometries. *J Mater Proc Technol* 240: 382–389. <https://doi.org/10.1016/j.jmatprotec.2016.10.008>
10. Zhang ZH, Dong SY, Wang YJ, et al. (2016) Study on microstructures and mechanical properties of super narrow gap joints of thick and high strength aluminum alloy plates welded by fiber laser. *Int J Adv Manuf Technol* 82: 99–109. <https://doi.org/10.1007/s00170-015-7334-5>
11. Fialko N, Prokopov V, Meranova N, et al. (1994) Temperature conditions of particle-substrate systems in a gas-thermal deposition process. *Fizika Khimiya Obrabot Mater* 2: 59–67. Available from: <https://www.scopus.com/pages/publications/0028385421?origin=resultslist>.
12. Li JG, Wang SQ (2017) Distortion caused by residual stresses in machining aeronautical aluminum alloy parts: Recent advances. *Int J Adv Manuf Technol* 89: 997–1012. <https://doi.org/10.1007/s00170-016-9066-6>
13. Ueda Y, Murakawa H, Ma N (2013) *Welding Deformation and Residual Stress Prevention*, Oxford: Butterworth-Heinemann. <https://doi.org/10.1016/C2011-0-06199-9>
14. Ibrak H, Abhijit B, Ashutosh P, et al. (2024) Computational investigation of plasma arc welding process for aluminium alloys. *Eng Res Express* 6: 025541 <https://doi.org/10.1088/2631-8695/ad4a24>
15. Makhnenko OV, Milenin OS, Muzhychenko OF, et al. (2023) Mathematical modeling of residual stress relaxation during performance of postweld heat treatment. *Paton Weld J* 6: 32–40. <https://doi.org/10.37434/tpwj2023.06.05>
16. Ma N, Deng D, Osawa N, et al. (2022) *Welding deformation and residual stress prevention*, 2 Eds, Oxford: Butterworth-Heinemann. <https://doi.org/10.1016/C2020-0-01663-4>
17. Goldak JA, Akhlaghi M (2005) Thermal analysis of welds, In: Goldak JA, Akhlaghi M, *Computational Welding Mechanics*, Boston: Springer, 71–117. [https://doi.org/10.1007/0-387-23288-5\\_3](https://doi.org/10.1007/0-387-23288-5_3)
18. Freire-Torres M, Carpio J (2023) Contribution to mathematical modeling and numerical simulation of welding processes, In: Vizán Idoipe A, García Prada JC, *Proceedings of the XV Ibero-American Congress of Mechanical Engineering. IACME 2022*, Cham: Springer. [https://doi.org/10.1007/978-3-031-38563-6\\_4](https://doi.org/10.1007/978-3-031-38563-6_4)
19. Klett J, Bongartz B, Wolf T, et al. (2023) Plasma welding of aluminum in an oxygen-free argon atmosphere. *Adv Mater Sci* 23: 5–18. <https://doi.org/10.2478/adms-2023-0001>
20. Fialko N, Prokopov V, Meranova N, et al. (1993) Thermal physics of gasothermal coatings formation processes. State of investigations. *Fizika Khimiya Obrabot Mater* 4: 83–93. Available from: <https://www.scopus.com/pages/publications/0027635013?inward=>.
21. Han YQ, Du MH, Yao QH, et al. (2011) The signal examination in variable polarity plasma arc welding of aluminum alloy. IEEE Third International Conference on Measuring Technology & Mechatronics Automation, 941–944. <https://doi.org/10.1109/ICMTMA.2011.807>
22. Prokopov V, Fialko N, Sherenkovskaya G, et al. (1993) Effect of the coating porosity on the processes of heat transfer under, gas-thermal atomization. *Powder Metall Met Ceram* 32: 118–121. <https://doi.org/10.1007/BF00560034>

23. Xu B, Chen S, Jiang F, et al. (2019) The influence mechanism of variable polarity plasma arc pressure on flat keyhole welding stability. *J Manuf Process* 37: 519–528. <https://doi.org/10.1016/j.jmapro.2018.12.026>
24. Wolczynski W, Okane T, Senderowski C, et al. (2011) Meta-stable conditions of diffusion brazing. *Arch Metall Mater* 56: 311–323. <https://doi.org/10.2478/v10172-011-0035-7>
25. Çevik B, Koç M (2019) The effects of welding speed on the microstructure and mechanical properties of marine-grade aluminium (AA5754) alloy welded using MIG welding. *Kovove Mater-Metall Mater* 57: 307–316. [https://doi.org/10.4149/km\\_2019\\_5\\_307](https://doi.org/10.4149/km_2019_5_307)
26. Tong H, Ueyama T, Ushio M (2002) Improvement of aluminium alloy sheet metal welding quality and productivity with AC pulsed MIG welding system (Report 2). *Weld Int* 16: 104–109. <https://doi.org/10.1080/09507110209549500>
27. Zhou YY, Liu HM, Yang YH, et al. (2025) Optimization of pulsed plasma arc welding parameters for high-quality joints in 2024 aluminum alloy thin sheets. *Mater Today Commun* 49: 113852. <https://doi.org/10.1016/j.mtcomm.2025.113852>
28. Tashiro S (2024) Interaction mechanism of arc, keyhole, and weld pool in keyhole plasma arc welding: A review. *Materials* 17: 1348. <https://doi.org/10.3390/ma17061348>
29. Olabode M, Kah P, Martikainen J (2013) Aluminium alloys welding processes: Challenges, joint types and process selection. *Proc Inst Mech Eng B J Eng Manuf* 227: 1129–1137. <https://doi.org/10.1177/0954405413484015>
30. Senderowski C, Cinca N, Dosta S, et al. (2019) The effect of hot treatment on composition and microstructure of HVOF iron aluminide coatings in Na<sub>2</sub>SO<sub>4</sub> molten salts. *J Therm Spray Technol* 28: 1492–1510. <https://doi.org/10.1007/s11666-019-00886-w>
31. Jittavisuttiwong P, Poopat B (2013) Effect of helium addition in argon shielding gas on metal transfer behavior in gas metal arc welding of aluminum. *Key Eng Mater* 545: 219–224. <https://doi.org/10.4028/www.scientific.net/KEM.545.219>
32. Fortain JM, Gadrey S (2013) How to select a suitable shielding gas to improve the performance of MIG and TIG welding of aluminium alloys. *Weld Int* 27: 936–947. <https://doi.org/10.1080/09507116.2012.753257>
33. Hakem M, Lebaili S, Mathieu S, et al. (2019) Effect of microstructure and precipitation phenomena on the mechanical behavior of AA6061-T6 aluminum alloy weld. *Int J Adv Manuf Technol* 102: 2907–2918. <https://doi.org/10.1007/s00170-019-03401-1>
34. Su D, Zhang J, Wang B (2020) The microstructure and weldability in welded joints for AA 5356 aluminum alloy after adding modified trace amounts of Sc and Zr. *J Manuf Process* 57: 488–498. <https://doi.org/10.1016/j.jmapro.2020.07.017>
35. Wang Y, Chen M, Wu C (2020) HF pulse effect on microstructure and properties of AC TIG butt-welded joint of 6061Al alloy. *J Manuf Process* 56: 878–886. <https://doi.org/10.1016/j.jmapro.2020.05.055>
36. Xue J, Xu M, Huang W, et al. (2019) Stability and heat input controllability of two different modulations for double-pulse MIG welding. *Appl Sci* 9: 127. <https://doi.org/10.3390/app9010127>
37. Liu J, Jiang F, Chen S, et al. (2023) Analysis of molten metal fluid flow mechanisms in variable polarity plasma arc welding of aluminum alloys. *Phys Fluids* 35: 092107. <https://doi.org/10.1063/5.0165380>

38. Xu B, Zhang C, Zhang G, et al. (2025) Metal flow mechanisms during alternating current arc welding and additive manufacturing of aluminium alloy. *Commun Mater* 6: 94. <https://doi.org/10.1038/s43246-025-00819-x>
39. Fialko N, Sherenkovskii J, Meranova N, et al. (2021) Establishing patterns in the effect of temperature regime when manufacturing nanocomposites on their heat-conducting properties. *East Eur J Enterp Technol* 112: 21–26. <https://doi.org/10.15587/1729-4061.2021.236915>
40. Dada M, Popoola P (2024) Recent advances in joining technologies of aluminum alloys: A review. *Discover Mater* 4: 86. <https://doi.org/10.1007/s43939-024-00155-w>
41. Han J, Shi Y, Guo JC, et al. (2023) Porosity inhibition of aluminum alloy by power-modulated laser welding and mechanism analysis. *J Manuf Process* 102: 827–838. <https://doi.org/10.1016/j.jmapro.2023.08.001>
42. Dai H, Shen X, Wang H (2018) Study on the arc pressure of TIG welding under the condition of Ar-Ar and Ar-He supply alternately. *Results Phys* 10: 917–922. <https://doi.org/10.1016/j.rinp.2018.08.015>
43. Fialko N, Dinzhos R, Sherenkovskii J, et al. (2021) Establishment of regularities of influence on the specific heat capacity and thermal diffusivity of polymer nanocomposites of a complex of defining parameters. *East Eur J Enterp Technol* 114: 34–39. <https://doi.org/10.15587/1729-4061.2021.245274>
44. Reinheimer EN, Weber R, Graf T (2022) Process limit imposed by the occurrence of undercuts during high-speed laser welding. *J Laser Appl* 34: 032003. <https://doi.org/10.2351/7.0000621>
45. Zhang Q, Yang C, Lin S, et al. (2015) Research on novel soft variable polarity plasma arc welding technology for aluminum alloys in horizontal position. *J Mech Eng* 51: 75–81. <https://doi.org/10.3901/JME.2015.24.075>
46. Zhang QL, Yang CL, Lin SB, et al. (2014) Horizontal welding of aluminium alloys by soft plasma arc. *Proc Inst Mech Eng B J Eng Manuf* 228: 1481–1490. <https://doi.org/10.1177/0954405413519435>
47. Yan Z, Chen S, Jiang F, et al. (2019) Study and optimization against the gravity effect on mechanical property of VPPA horizontal welding of aluminum alloys. *J Manuf Process* 46: 109–117. <https://doi.org/10.1016/j.jmapro.2019.08.028>
48. Huang Y, Zhang Z, Lv N, et al. (2015) On the mechanism and detection of porosity during pulsed TIG welding of aluminum alloys. *Adv Intell Syst Comput* 363: 133–143. [https://doi.org/10.1007/978-3-319-18997-0\\_11](https://doi.org/10.1007/978-3-319-18997-0_11)
49. Fialko N, Dinzhos R, Sherenkovskaya G, et al. (2022) Influence on the thermophysical properties of nanocomposites of the duration of mixing of components in the polymer melt. *East Eur J Enterp Technol* 116: 25–30. <https://doi.org/10.15587/1729-4061.2022.255830>
50. Cui N, Zhao T, Wang Z, et al. (2025) Porosity evolution mechanisms, influencing factors, and ultrasonic-assisted regulation in joining high Mg-content aluminum alloys. *J Mater Process Technol* 336: 118706. <https://doi.org/10.1016/j.jmatprotec.2024.118706>
51. Wolczynski WS, Okane T, Senderowski C, et al. (2011) Thermodynamic justification for the Ni/Al/Ni joint formation by diffusion brazing. *Int J Thermodyn* 14: 97–105. <https://doi.org/10.5541/ijot.296>
52. Fox S, Campbell J (2000) Visualisation of oxide film defects during solidification of aluminium alloys. *Scripta Mater* 43: 881–886. [https://doi.org/10.1016/S1359-6462\(00\)00506-6](https://doi.org/10.1016/S1359-6462(00)00506-6)

53. Ardika RD, Triyono T, Muhayat N, et al. (2021) A review porosity in aluminum welding. *Procedia Struct Integr* 33: 171–180. <https://doi.org/10.1016/j.prostr.2021.10.021>
54. Trometer N, Chen B, Moodispaw M, et al. (2024) Modeling and validation of hydrogen porosity formation in aluminum laser welding. *J Manuf Process* 124: 877–890. <https://doi.org/10.1016/j.jmapro.2024.06.052>
55. Senderowski C, Bojar Z, Wolczynski W, et al. (2007) Residual stresses determined by the modified Sachs method within a gas detonation sprayed coatings of the Fe-Al intermetallic. *Arch Metall Mater* 52: 569–578.
56. Lang R, Han Y, Ma Y (2025) Impact of welding current on weld formation in variable polarity plasma arc welding: A numerical and experimental analysis. *Materials* 18: 1122. <https://doi.org/10.3390/ma18051122>
57. Skorokhod AZ, Sviridova IS, Korzhik VN (1995) The effect of mechanical pretreatment of polyethylene terephthalate powder on the structural and mechanical properties of coatings made from it. *Mech Compos Mater* 30: 328–334.
58. Lang R, Han Y, Bao X, et al. (2023) Stability mechanism of the molten pool in variable polarity plasma arc welding of medium thickness aluminum alloy. *J Mater Process Technol* 321: 118127. <https://doi.org/10.1016/j.jmatprotec.2023.118127>
59. Yan Z, Chen S, Jiang F, et al. (2018) Material flow in variable polarity plasma arc keyhole welding of aluminum alloy. *J Manuf Process* 36: 480–486. <https://doi.org/10.1016/j.jmapro.2018.10.023>
60. Jiang F, Li C, Chen S (2019) Experimental investigation on heat transfer of different phase in variable polarity plasma arc welding. *Weld World* 63: 1153–1162. <https://doi.org/10.1007/s40194-019-00722-3>
61. Mahadevan G, Senthilkumar T, Ramasamy N (2023) GMA welding investigations on the effect of alternating shielding gases on bead profile characteristics of AA6061 aluminum alloy. *J Process Mech Eng* 238: 1836–1850. <https://doi.org/10.1177/09544089231173215>
62. Zhang QL, Yang CL, Lin SB, et al. (2015) Soft variable polarity plasma arc horizontal welding technology and weld asymmetry. *Sci Technol Weld Join* 20: 297–306. <https://doi.org/10.1179/1362171815Y.0000000006>
63. Senderowski C, Pawlowski A, Bojar Z, et al. (2010) TEM microstructure of Fe-Al coatings detonation sprayed onto steel substrate. *Arch Metall Mater* 55: 373–381. Available from: <https://repo.bg.wat.edu.pl/info/article/WAT6ff5935e56ea4811a8fbf4f3e376a239/>.
64. Liu J, Jiang F, Tashiro S, et al. (2024) The mechanism of dual-stagnation points flow phenomenon in keyhole plasma arc melt pool and corresponding control strategy. *J Manuf Process* 125: 473–488. <https://doi.org/10.1016/j.jmapro.2024.07.078>
65. Lang R, Han Y, Bai X, et al. (2022) Influence of the metal flow in the keyhole molten pool on the molten pool stability in continuous variable polarity plasma arc keyhole vertical-up welding. *J Manuf Process* 76: 195–209. <https://doi.org/10.1016/j.jmapro.2021.12.052>
66. Chen G, Sun Y, Wang C, et al. (2025) Characterising and modelling plasma transferred arc for additive manufacturing. *Int J Heat Mass Transf* 241: 126735. <https://doi.org/10.1016/j.ijheatmasstransfer.2025.126735>
67. Momin AG, Khatri BC, Chaudhari M, et al. (2022) Parameters for cladding using plasma transfer arc welding—A critical. *Mater Today Proc* 77: 614–618. <https://doi.org/10.1016/j.matpr.2022.11.009>



68. Chandima Ratnayake RM (2014) A methodology for assessing most vulnerable welding procedure specifications and imperfection factors. *Int J Data Anal Tech Strat* 6: 362–383. <https://doi.org/10.1504/IJDATS.2014.066606>
69. Skorokhod AZ, Sviridova IS, Korzhik VN (1994) Structural and mechanical properties of polyethylene terephthalate coatings as affected by mechanical pretreatment of powder in the course of preparation. *Mekhanika Kompozit Mater* 30: 455–463.
70. Karayel E, Bozkurt Y, Özdemir C, et al. (2022) Wire arc additive manufacturing of 5356 aluminum alloy. *Res Sq*. <https://doi.org/10.21203/rs.3.rs-1529479/v2>
71. Novianto E, Iswanto PT, Mudjijana M (2018) The effects of welding current and purging gas on mechanical properties and microstructure of tungsten inert gas welded aluminum alloy 5083 H116. *MATEC Web Conf* 197: 12007. <https://doi.org/10.1051/mateconf/201819712007>
72. Liu Y, Liu J, Ye H, et al. (2019) Study on plasma arc welding technology and properties of metal materials. *IOP Conf Ser Mater Sci Eng* 563: 022003. <https://doi.org/10.1088/1757-899X/563/2/022003>
73. Vakili-Tahami F, Ziaei-Asl A (2013) Numerical and experimental investigation of T-shape fillet welding of AISI 304 stainless steel plates. *Mater Des* 47: 615–623. <https://doi.org/10.1016/j.matdes.2012.12.064>
74. Song S, Ahn S, Kim Y, et al. (2015) Development of simplified finite element models for welded joints. *Trans Korean Soc Mech Eng A* 39: 1191–1198. <https://doi.org/10.3795/KSME-A.2015.39.11.1191>
75. Cho H, Nam S, Kang M, et al. (2020) Predicting failure modes of resistance spot welds from the chemical composition of materials. *J Weld Join* 38: 450–459. <https://doi.org/10.5781/JWJ.2020.38.5.4>
76. Lee TS, Lee HY, Shin SJ (1998) An estimative model of spot weld failure-1. Failure criteria. *Trans Korean Soc Autom Eng* 6: 40–52. Available from: <https://www.koreascience.or.kr/article/JAKO199822452069038.page>.
77. Askeland DR, Fulay PP (2009) *Essentials of Materials Science and Engineering*. 2 Eds., Toronto: Cengage Learning, 185–205. Available from: <https://ftp.idu.ac.id/wp-content/uploads/ebook/tdg/TEKNOLOGI%20REKAYASA%20MATERIAL%20PERTAHANAN/Askeland-Essentials-of-Materials-Science-and-Engineering-1.pdf>.
78. Liu ZM, Cui SL, Luo Z, et al. (2016) Plasma arc welding: Process variants and its recent developments of sensing, controlling and modeling. *J Manuf Process* 23: 315–327. <https://doi.org/10.1016/j.jmapro.2016.04.004>
79. Jiang F, Li W, Xu B, et al. (2024) Variable polarity plasma arc welding: Process development and its recent developments of detecting, modeling, and controlling. *J Manuf Process* 114: 1–17. <https://doi.org/10.1016/j.jmapro.2024.01.078>
80. Hung Ha M, Vu D, Tinh Do H (2023) Experimental design in plasma welding of SUS 304 stainless steel thin plates. *J Pengabdian Kepada Masy Teknol Appl* 4. <https://doi.org/10.12928/spekta.v4i1.7864>
81. Maksimova SV, Khorunov VF, Myasoed VV, et al. (2014) Microstructure of brazed joints of nickel aluminide. *Paton Weld J* 10: 15–21. <https://doi.org/10.15407/tpwj2014.10.03>
82. Şahin EI, Emek M, Ibrahim JEFM (2023) *Instrumental Measurements Laboratory*, Iksad: Publishing House, 80. <https://doi.org/10.5281/zenodo.12759673>

83. ISO 10042:2018. Welding—Arc-welded joints in aluminium and its alloys—Quality levels for imperfections. Available from: <https://www.iso.org/standard/70566.html>.
84. Kakade S, Thakur A, Patil S, et al. (2023) Experimental evaluation and correlation of plasma transferred arc welding parameters with hardfacing defects. In: Gupta R, Deshmukh D, Patil AP, et al. *Recent Advances in Material, Manufacturing, and Machine Learning*, London: CRC Press, 326–331. <https://doi.org/10.1201/9781003358596-34>
85. Lang R, Han Y, Bai X, et al. (2022) Impacting mechanism of variable polarity frequency on weld pool stability in variable polarity plasma arc keyhole vertical welding of aluminum alloy. *Rare Met Mater Eng* 51: 1172–1182. <https://doi.org/10.12442/j.issn.1002-185X.20210102>
86. Dai H, Miao J, Lin J (2024) Grain refinement of 5A06 aluminum alloy welds caused by tungsten inert gas welding arc characteristics under Ar–He alternating gas supply conditions: A coupled method of water-cooled copper plate test/numerical simulation. *J Iron Steel Res Int* 31: 767–777. <https://doi.org/10.1007/s42243-023-01120-2>
87. Ishchenko AYa, Budnik VP, Poklyatsky AG, et al. (2000) Effect of composition of shielding gases on technological characteristics of arc during non-consumable electrode welding of aluminium alloys. *Paton Weld J* 2: 17–20. Available from: <https://patonpublishinghouse.com/ukr/journals/tpwj/2000/02>.



AIMS Press

© 2025 the Author(s), licensee AIMS Press. This is an open access article distributed under the terms of the Creative Commons Attribution License (<https://creativecommons.org/licenses/by/4.0>)